Urban Climate 25 (2018) 167–186

Contents lists available at ScienceDirect

Urban Climate

journal homepage: www.elsevier.com/locate/uclim

Evaluating the local climate zone classification in high-density heterogeneous urban environment using mobile measurement

Yuan Shi[a,*], Kevin Ka-Lun Lau[b,c,d], Chao Ren[a,b,c], Edward Ng[a,b,c]

[a] School of Architecture, The Chinese University of Hong Kong, Shatin, N.T., Hong Kong Special Administrative Region
[b] The Institute of Environment, Energy and Sustainability (IEES), The Chinese University of Hong Kong, Shatin, N.T., Hong Kong Special Administrative Region
[c] Institute Of Future Cities (IOFC), The Chinese University of Hong Kong, Shatin, N.T., Hong Kong Special Administrative Region
[d] CUHK Jockey Club Institute of Ageing, The Chinese University of Hong Kong, Shatin, N.T., Hong Kong Special Administrative Region

ARTICLE INFO

Keywords:
Urban heat island
Local climate zone (LCZ)
World urban database and access portal tools (WUDAPT)
Mobile measurement
High-density city
Hong Kong

ABSTRACT

Urban heat island (UHI) has been identified as a threat to urban living quality in the context of climate change. As awareness of the impacts of urban expansion on local climate increases, urban planners/decision makers attempt to incorporate climatic considerations into the planning process. An increasingly-used urban climatic analysis scheme— Local Climate Zone (LCZ) classification— has been applied in Hong Kong, a high-density city with heterogeneous an urban environment. This study aims to evaluate the LCZ mapping in such a unique urban context using in-situ air temperature data. The fine-scale spatial variation of the daytime and nighttime screen-level air temperatures was investigated via mobile measurements during the summertime of 2016. The measured data were collated in Geographic Information System (GIS) based on the current LCZ maps. Statistically significant air temperature differences were observed between most LCZ classes, which confirm the veracity of LCZ in high-density heterogeneous urban contexts. Higher uncertainties in the site-averaged air temperature and considerable intra-LCZ air temperature differences in LCZs 1 to 6 were observed. It indicates that the current LCZ procedures of Hong Kong can be further refined for a better understanding of the climatic heterogeneity in densely built urban areas.

1. Introduction

Extreme weather events, such as heat waves, are becoming more frequent and intense amid climate change (IPCC 2014). Such trend will have a tremendous effect on health (McMichael, Woodruff, and Hales 2006, WHO 2003), particularly in highly urbanized and sprawling cities (Stone, Hess, and Frumkin 2010). Furthermore, due to the Urban Heat Island (UHI) phenomenon in highly urbanized areas, the impact of heat wave could be further intensified (Tan et al. 2010). As one of the densest and most populated cities in the world, Hong Kong is particularly susceptible to severe heat-related health consequences (Chan et al. 2012). Traditionally, the UHI intensity is described as the air temperature difference between the urban area and its surrounding rural areas (Rizwan, Dennis, and Liu 2008). However, under a heterogeneous urban context, this definition is inadequate to depict the intra-urban differences in air temperature between different districts in a large city (Chen et al. 2012, Stewart and Oke 2012, Oke 2004, Lowry 1977).

Urban form is closely related to the urban climate (Eliasson 1990). The forms of urban planning and development are influential

* Corresponding author at: Rm905, YIA Building, The Chinese University of Hong Kong, Shatin, NT, Hong Kong Special Administrative Region.
E-mail address: shiyuan@cuhk.edu.hk (Y. Shi).

https://doi.org/10.1016/j.uclim.2018.07.001
Received 26 November 2017; Received in revised form 12 June 2018; Accepted 1 July 2018

to the local climatic conditions (Grimmond 2007) because the urban environment alters the wind flow, radiation balance, water and heat balances (Landsberg 1981). Urban expansion without appropriate planning control leads to substantial environmental degradation (Betanzo 2007). As awareness of the impacts of urban expansion on local climate grows, urban planners and decision makers have started to incorporate the climatic consideration into the planning process (Eliasson 2000).

To provide a better spatial understanding of local climate and help planners improve the urban form based on the climatic consideration, several classification schemes have been developed. They are the Urban Zones of Energy partitioning (UZE) (Loridan and Grimmond 2012, Loridan et al. 2013), Urban Climatic Map (UCMap) system (Ren, Ng, and Katzschner 2011), Urban Climate Zone (UCZ) scheme (Oke 2004, 2006) and Local Climate Zone (LCZ) scheme (Stewart and Oke 2012). The common theme of these different schemes is that all of them are established according to the information from urban indicators. These urban indicators include but are not limited to the land use/land cover (LU/LC) pattern, topographic, surface geometry and climatic spatial information. Based on this information, the above mentioned zoning systems/schemes can depict the effects of the spatially varied urban environment on local climate modifications. Urban form and function classification are standardized in the LCZ scheme, making it possible to provide a more detailed spatial understanding of the variability of intra-urban air temperature, rather than a simple description of urban-rural difference (Stewart and Oke 2012). The LCZ scheme was developed and serves as a global standard for depicting different urban morphologies (Stewart and Oke 2009). The scheme features 17 types of LCZ classes, including ten built types (LCZ 1 to LCZ 10), and seven land cover types (LCZ A to LCZ G). A full list of LCZ classes is shown in.

The properties of each LCZ class can be differentiated by metadata of urban land use and morphological factors (Stewart and Oke 2012). LCZs generated following the highly standardized scheme can help examine the UHI phenomenon in different cities. The advantage of the LCZ scheme over tradition land-use classification methods is that it also takes urban morphological details into consideration, which advances urban climatic research. Therefore, LCZ has been used in many different cities around the world for mapping (Bechtel et al. 2015). Moreover, to generate an internationally standardized LCZ classification database, a new project —World Urban Database and Access Portal Tools (WUDAPT)— was initiated in 2012 (Mills et al. 2015). It aims to develop LCZ maps for cities where detailed urban morphological data are not available using open-source remote sensing data. The performance of WUDAPT data in urban climatic analysis and the subsequent urban planning processes, in terms of accuracy and relevance, therefore requires comprehensive assessment (Stewart, Oke, and Krayenhoff 2014).

In Hong Kong, a prior study has classified 17 weather stations in the weather monitoring network of the Hong Kong Observatory (HKO) into LCZ scheme for UHI quantification (Siu and Hart 2012). After that, to develop climate-adapted urban planning and design strategies for the local practice, another study has further developed an LCZ classification map (with a spatial resolution of 300 m) for Hong Kong—a high-density large city with a highly heterogeneous urban environment (Zheng et al., 2018). The study's mapping method was GIS-based and it was possible because sufficient and detailed data of urban indicators are available in Hong Kong from the local planning department (PlanD). A set of LCZ maps with a finer spatial resolution of 100 m (a WUDAPT level 0 product) was also developed using the WUDAPT method to align the LCZ map of Hong Kong with worldwide research (Ren et al. 2016). The mapping accuracy of both of the above studies was evaluated in the study of Wang et al. (2018). The spatial pattern of the resultant LCZ maps showed a high consistency with the previous UCMaps system of Hong Kong. However, intra-LCZ site variations of urban indicators were also detected in the built-up LCZ classes (particularly LCZ1-6, see.

Table 1 and Fig. 1) of the resultant maps. It confirms the necessity of validation using measured air temperature data. The above also indicates the potential of further optimization of the LCZ classification procedure in a high-density urban scenario.

Mobile measurement using moving vehicles has been regarded a cost-effective method to investigate intra-urban environmental variability (Peters, Van Poppel, and Theunis 2012, Peppler 1929). It fills the monitoring gaps of the sparsely distributed fixed monitoring locations by providing more spatial information. This method has been increasingly adopted and continuously improved

Table 1
Criteria for GIS-based classification of LCZs in Hong Kong. Values for LCZs 1 to 9 are from Stewart and Oke (2012). Criteria for LCZs 10 to G are adapted from local urban planning datasets of Hong Kong (Wang et al., 2018).

LCZ Classes	Criteria of Classification
LCZ 1-Compact High-rise	$0.4 < \lambda_b < 0.6$ and $Z_h > 25$
LCZ 2-Compact Mid-rise	$0.4 < \lambda_b < 0.7$ and $10 < Z_h < 25$
LCZ 3-Compact Low-rise	$0.4 < \lambda_b < 0.7$ and $3 < Z_h < 10$
LCZ 4-Open High-rise	$0.2 < \lambda_b < 0.4$ and $Z_h > 25$
LCZ 5-Open Mid-rise	$0.2 < \lambda_b < 0.4$ and $10 < Z_h < 25$
LCZ 6-Open Low-rise	$0.2 < \lambda_b < 0.4$, $3 < Z_h < 10$
LCZ 7-Lightweight Low-rise	$0.6 < \lambda_b < 0.9$, $2 < Z_h < 4$, $0.2 < \Psi_{svf} < 0.5$
LCZ 8-Large Low-rise	$0.3 < \lambda_b < 0.5$, $3 < Z_h < 10$, $\Psi_{svf} > 0.7$
LCZ 9-Sparsely Built	$0.1 < \lambda_b < 0.2$, $3 < Z_h < 10$, $\Psi_{svf} > 0.8$
LCZ 10-Heavy Industry	LU/LC = Industrial Land
LCZ A-Dense Trees	LU/LC = Woodland
LCZ B-Scattered Trees	(LCZ A/B were combined due to the lack of information on wood species.)
LCZ C-Bush, Scrub	LU/LC = Shrub Land
LCZ D-Low Plants	LU/LC = Agricultural Land
LCZ *E*-Bare Rock or Paved	LU/LC = Roads, Railway, Airport, Quarries, Rocky Shore
LCZ F-Bare Soil or Sand	LU/LC = Badland, Vacant Development Land/Construction in Progress
LCZ G-Water	LU/LC = Reservoirs, Streams and Nullahs

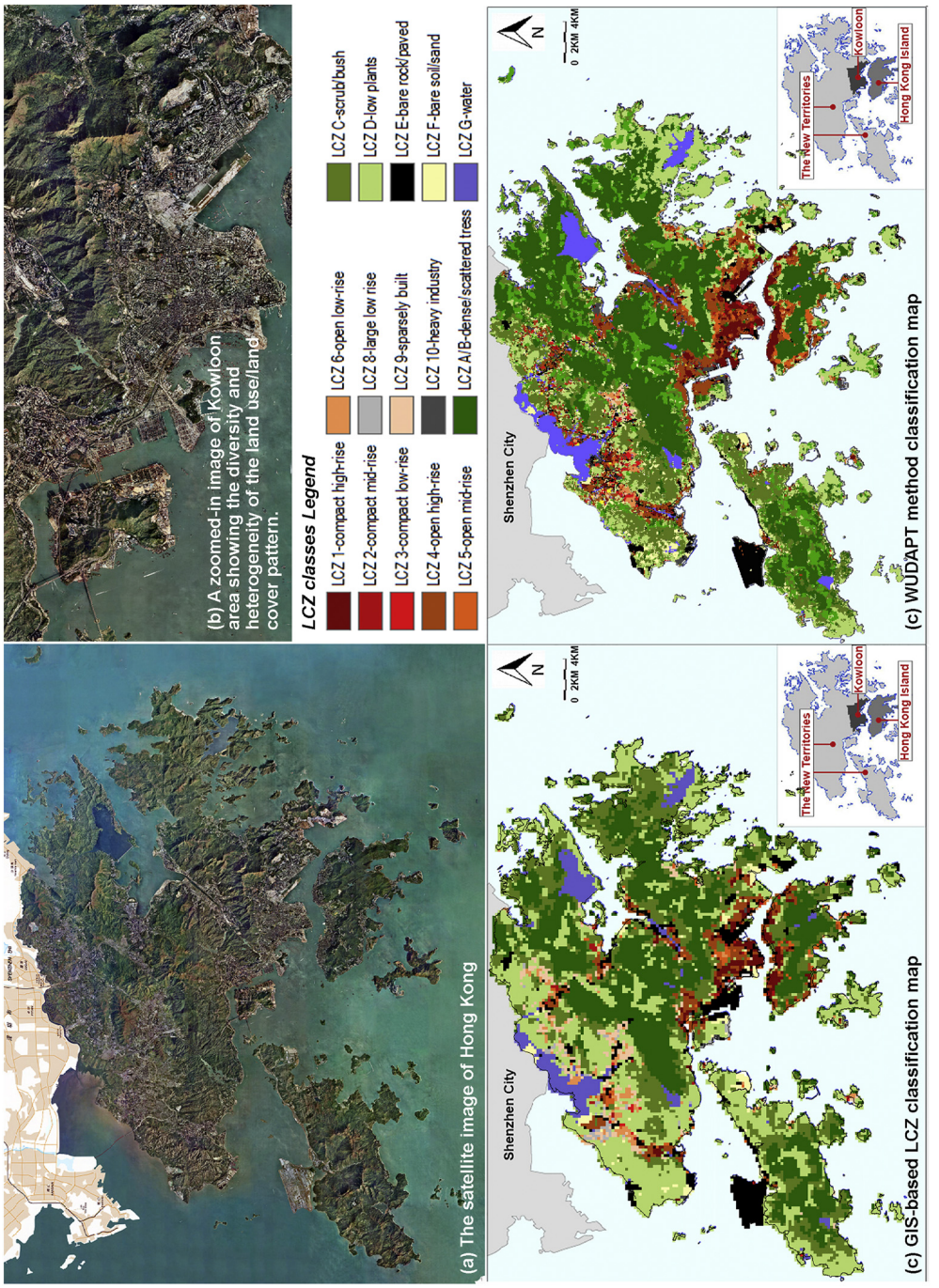

Fig. 1. The satellite images - (a) and (b), current GIS-based LCZ map (c) (Zheng et al., 2018), and WUDAPT map (d) (Wang et al., 2018) of Hong Kong.

in UHI investigation (Liu et al. 2016, Tsin et al. 2016, Stewart 2011). Air temperature data acquired by the mobile measurement method have been used for many different study purposes. For example, they were employed to characterize the urban-rural air temperature difference (Hedquist and Brazel 2006, Unger, Sümeghy, and Zoboki 2001), correlate urban air temperature with remotely sensed land surface temperature (LST), understand the relationship between the microclimate condition and urban geometry (Blankenstein et al., 2004, Tsin et al. 2016), and evaluate the cooling effects of urban greenery (Lu et al. 2012). In Hong Kong, a few prior air temperature studies have made use of mobile measurement in both urban built-up and rural areas (Nichol et al. 2009, Zheng et al. 2015). The success of these studies confirms the feasibility of monitoring microscale spatial variation of air temperature and the potential of validating further studies using the mobile measurement method.

Recently, the mobile measurement method has gained popularity and success in LCZ classification and spatialization studies (Szymanowski and Kryza 2009, Alexander and Mills 2014). Observation-based LCZ studies are normally based on urban meteorological networks (Skarbit et al. 2017, Lehnert et al. 2015, Unger et al. 2015). The fixed monitoring networks work well in mid-density cities in Europe and North America that are more uniformly developed with discreet patterns of land use and urban form. However, the geographic setting and urban contexts of many densely populated large cities (especially in Asia) are more heterogeneous and complex. Such geographic complexity with mixed forms results in large air temperature variations between and within different LCZ classes of the city at a relatively smaller spatial scale. Such spatial variations cannot be effectively investigated by fixed monitoring networks alone. To evaluate LCZ classification/mapping, a comprehensive understanding of the spatial variation of air temperature needs to be acquired. The spatial advantages of mobile measurement make it ideal for investigating the relationship between the urban built-up surface and the near-surface air temperature. Therefore, the mobile measurement method has been further applied in the evaluation of the LCZ-based UHI assessment (Leconte et al. 2015, Kotharkar and Bagade 2018).

The mobile platform is particularly useful in the investigation of the screen-level environmental variation in Hong Kong because of its unique urban environment (Shi, Lau, and Ng 2016). Previous mobile measurement case cities in North America and European have been done in a relatively simple urban context that shows more uniformly discreet patterns of land use and urban form. However, downtown areas in Hong Kong are high-density high-rise and their urban context is highly inhomogeneous in terms of urban morphology and mixed land use at local scales. Its extreme heterogeneity and high-density high-rise environment can possibly lead to a large difference between the ambient air temperature measured by the fixed monitoring locations in the network of HKO weather stations and the screen-level air temperature via mobile measurement. The consideration is particularly important in the street canyons of the high-density downtown area. Under such circumstance, the screen-level air temperature measured using the mobile platform has a better potential to reflect the actual situation of people's outdoor heat exposure and is more informative to UHI investigation and health impact assessments.

This study uses mobile measurement to evaluate the performance of the current LCZ mappings (results from both the GIS-based method and WUDAPT method) of Hong Kong in determining the spatial variation of UHI and informing urban climatic studies. In the present study, air temperature differences between LCZ classifications and the intra-LCZ temperature variability were extracted from the mobile measurement data set. Further assessments were then conducted for the current LCZ mapping schemes of Hong Kong. The study results indicate that LCZ measurement and mapping systems in Hong Kong could be optimized through some improvement strategies.

2. Materials, methods, and study area

2.1. The geographic and urban context of Hong Kong

Hong Kong is a subtropical city located on the southeast coast of China (22° 150′ N, 114° 100′ E. Fig. 3 shows the location). Its subtropical maritime weather features hot humid summer with occasional showers and thunderstorms and warm winter. Hong Kong has abundant natural green resources, a hilly topography, coastal landscapes and diverse geological features in its countryside. > 70% of land (measuring approximately 1100 km^2) is vegetated mountainous areas and country parks (Taylor 1986). Only less than a quarter of the land resources in regions with a relatively flat topography and at a lower elevation are used for urban development (PlanD 2015). The complex urban morphology due to mixed land use is primarily due to the geographical constraints and urban development oriented to major transportation corridors. Urban centres were developed along transportation nodes and are self-sustained in nature. As such, land utilization is characterized by the diverse nature. In addition, the large population requires a high-density and high-rise mode of development. Both natural and artificial land cover types in Hong Kong are very diverse. The mixture of different landscapes shapes the unique urban context of Hong Kong (Fig. 1-a, b).

2.2. Current LCZ classification and spatial map of Hong Kong

2.2.1. GIS-based mapping

As mentioned, a GIS-based LCZ classification has been developed for high-density Hong Kong. The criteria are described as follows (Zheng et al., 2018):

First, built-up classes and land cover classes were separated by reclassifying the land use data of Hong Kong. Then, for built-up classes (LCZ 1 to LCZ 10), LCZ 10 was identified based on the industrial land use type, and LCZ 1 to LCZ 9 were quantitatively differentiated based on three building morphological factors - building surface fraction (λ_b, [0–1]), building height (Z_h, unit: m), and sky view factor (Ψ_{svf}, [0–1]). Stewart and Oke (2012) proposed a set of standard values of geometric and surface cover properties for LCZs. Among them, four parameters are about the urban surface roughness - canyon aspect ratio (H/W) and λ_b, Z_h, terrain roughness

class. Instead of including all morphological factors, only three key factors were used as parameters for the LCZ classification in this study. For example, Ψ_{svf} is essentially correlated with H/W (Oke 1981). Moreover, it has been tested that the Ψ_{svf} is a very good indicator of intra-urban air temperature differentials in the high-rise high-density urban areas of Hong Kong (Chen et al. 2012). Therefore, Ψ_{svf} was used. The criteria for terrain roughness class were set up based on the Davenport et al. (2000)'s classification, which is not suitable for depicting high-density urban morphology [most of the built-up areas can only be classified into Class 8 "Skimming: City center ($z_0 \geq 2$)"] (Ng et al. 2011). Therefore, we used Z_h for the classification. All building morphological factors were calculated and mapped at a spatial resolution of 100 m.

Table 1 shows the quantitative classification scheme of the built-up classes. For rural areas, a total of seven land cover classes (LCZ A - G) were further classified based on the land use type. The finalized LCZ map of Hong Kong is shown in Fig. 1-c. It has been found that LCZ classification results are often sensitive to the spatial scale of the LCZ site or mapping resolution, especially in Asia cities due to their unique urban contexts and heterogeneous urban environment (Kotharkar and Bagade 2017). Therefore, it is necessary to determine an appropriate spatial size of LCZ site before LCZ mapping. The map was produced at a spatial resolution of 300 m— the optimal spatial size of the LCZ site of Hong Kong according to Lau, Ren, et al. (2015). It should be noted that LCZ 7 and LCZ 8 were not detected by the GIS-based method, probably due to the extremely small areal proportion. The areas of LCZ 7 and LCZ 8 detected by WUDAPT method were quite small as well (1.22 km^2 and 1.08 km^2).

2.2.2. WUDAPT mapping

Unlike the GIS-based LCZ classification method, the WUDAPT level 0 mapping product follows a set of standard procedures for data collection and processing (See et al. 2015). Following the procedure described by Bechtel et al. (2015), Landsat 8 satellite images from the United States Geological Survey (USGS) were chosen as the data source for the WUDAPT mapping of Hong Kong. Using the method of visual interpretation, training samples were selected to represent each LCZ class with the help from urban planning experts familiar with the urban context of Hong Kong. WUDAPT identifies LCZ classes by random forest algorithm. This machine learning algorithm builds a decision tree based on the spectral features/patterns contained by the training samples. As a result, the WUDAPT level 0 map at a finer spatial resolution of 100 m was produced (Fig. 1-d).

2.3. Measuring screen-level air temperature using mobile platform

In this present study, mobile measurement campaigns were conducted during the summertime of the year of 2016. The spatial distribution of both the daytime and nighttime screen-level air temperature was investigated. The measured air temperature data were collated with the current LCZ classifications/WUDAPT maps of Hong Kong.

2.3.1. Mobile measurement platform

A light-colored Toyota bB mini MPV vehicle installed with microclimate sensors was used as the mobile platform for all measurement campaigns in this present study (Fig. 2 and Table 2). The air temperature (T_a, °C) and relative humidity (RH, %) were measured and logged at a time interval of one second using TESTO™ 480 Thermometers with the sensor - Humidity and Temperature

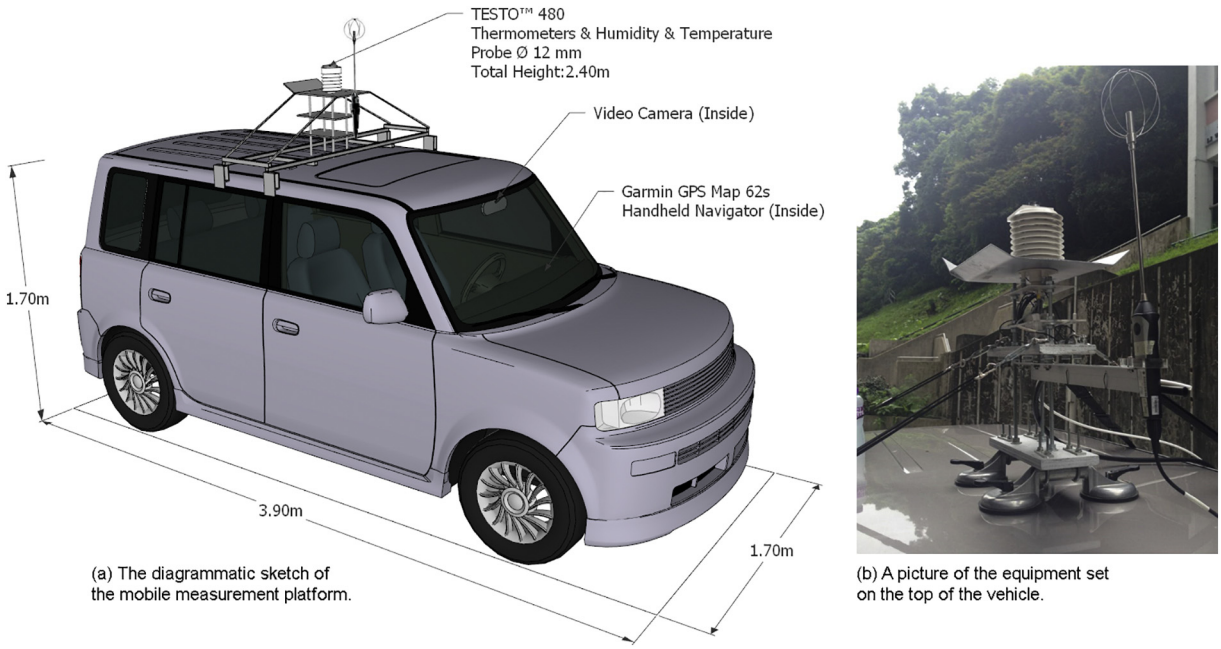

Fig. 2. The mobile measurement platform.

Table 2
Summary of measurement equipment installed on the mobile measurement platform.

Installed instruments	Measured parameter	Measuring interval	Accuracy of the instruments	Data category
TESTO™ 480 Thermometers & Humidity and Temperature Probe Ø 12 mm	Air temperature (T_a, °C) & Relative humidity (RH, %)	1 s (1 Hz frequency-measurement)	T_a: ± 0.3 °C (−20 to +70 °C) RH: ± 2% (2 to 98%)	Meteorological data
Garmin™ GPS Map 62 s Handheld Navigator	Latitude, Longitude, Altitude	1 s (1 Hz frequency-measurement)	Error within ± 3.7 m (12Feet)	GPS data
Video Camera	Driving video records	30FPS	N.A.	Referential video records

Probe Ø 12 mm. The geographical position of each measurement was simultaneously recorded with a Garmin™ GPS Map 62 s Handheld Navigator. A wide-angle video camera was installed at the front windshield of the vehicle to continuously record the surroundings during the entire process of each measurement campaign, providing a reference for the identification of any other influential factors of the temperature and humidity measurements. All microclimate sensors used in the mobile measurement were calibrated before the mobile measurement campaigns. They were solely used for the mobile measurement in this study and were maintained appropriately by professional technicians to ensure reliability.

2.3.2. Protocols of the mobile measurement campaigns

Two measurement routes with a total length of approximately 90 km were designed to cover a broad range of LCZ sites (Fig. 3). The length of route-1 was 35 km, and route-2 was 55 km. Route-1 covered more built-up areas, while route-2 passed through more land cover classes. The routes were also designed based on the areal proportion of different LCZ classes. As a result, the composition of the route length in different LCZ classes is proportional to the areal proportion of different classes in the LCZ map mentioned above (Fig. 4). Most of the built-up urban areas of Hong Kong are in regions with a relatively flat topography and at a lower elevation (The mean elevation is approximately 24 m. Most of the built-up areas is below the elevation of 60 m. See Fig. 3). Therefore, hilly areas were also avoided during the design of the mobile measurement routes. The elevation of most parts of the two routes approximately ranged from 10 m to 60 m without steep slopes. Moreover, most parts of the routes were far from the coastline with a distance of larger than 1000 m. The few road segments closer to the coastline were approximately 100 m to 200 m from it. A couple of pilot tests were conducted before the mobile measurement campaigns to make sure that both routes could be completed within 2 h. This time limit was set to minimize the spatial uncertainties in the data introduced by changes in the background weather conditions.

A total of 12 runs of the mobile measurement were completed under the typical hot weather condition of Hong Kong (Table 3). The T_a and RH of the days for measurement approximately ranged from 29 °C to 34 °C and 60% to 80% respectively. The sky condition measured as cloudiness (Oktas, 0-clear sky to 8-overcast) was also recorded. Three time periods of a day were measured to investigate the difference in the spatial variation in air temperature in different stages of a diurnal cycle.

2.3.3. Mobile measurement data processing and data analysis

Although we have controlled the time period of each measurement to avoid significant background weather changes, the effect of temporal trend of T_a and RH should be removed from the spatially distributed data. As the meteorological data from HKO are only available on an hourly basis, we performed a linear detrending for each hour of the period of measurements to remove the temporal effect in the measurement data based on literature (Comrie 2000, Jonsson 2004). As shown in Fig. 3, there are several HKO weather stations close to the two measurement routes. Firstly, a 1 Hz-temporally resolved linear trend was generated to represent the background weather changes at each station during each measurement run. Then, the 1 Hz frequency-measured data points of T_a and RH were separated into different partitions based on their corresponding closest HKO weather station. Temporal correction was then conducted for each data partition using their corresponding time period based on the 1 Hz-temporally resolved linear trend mentioned above. Based on the background meteorological records shown in Table 3, a day-to-day temporal correction was also performed to remove the temporal difference between the two mobile measurement routes.

To avoid the influence of the anthropogenic heat from vehicular exhaust, and to make the results of present study comparable with other LCZ/WUDAPT mobile measurement studies, all measurement data corresponding to a driving speed < 15 km/h or > 60 km were excluded from the dataset (the driving speed at each second was calculated in GIS). The driving speed criteria used here are consistent with a previous mobile measurement study in France (Leconte et al. 2015). Streets in Hong Kong, with its compact urban form, are often occupied by intense traffic and other activities. Under such context, some abnormal data points influenced by anomalous heat sources and sinks were observed in our measurement data. These abnormal data show up as spikes in the measurement data sequence. For example, there were abnormally high T_a observations (with a $T_a > 35$ °C lasting a few seconds during the nighttime measurement) caused by a suddenly passing-by heavy-duty truck or a double-decker bus emitting a large amount of the vehicular heat exhaust. We also observed some cool spots in the measurement data (with a $T_a < 25$ °C in the afternoon) caused by the cool airflow from the air conditioners in roadside shops. These data were screened out before further analysis was conducted. In this study, we used a median filter to remove the spikes mentioned above.

A median filter is a nonlinear filtering algorithm widely used for noise reduction in the data sequence. It eliminates unwanted spikes in the signal without blurring any features of the original data sequence (Huang, Yang, and Tang 1979). This makes the median

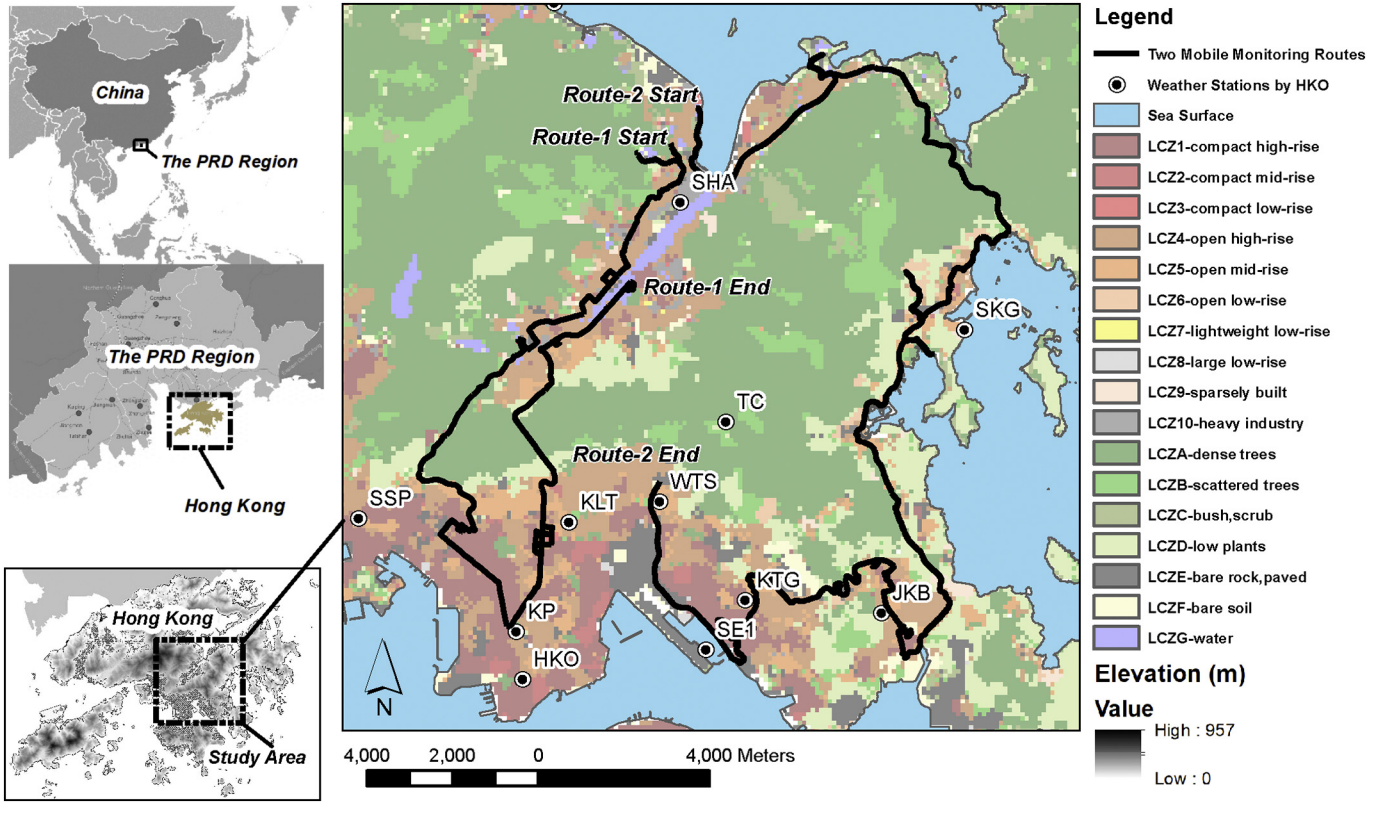

Fig. 3. The two routes designed for the mobile measurement of the screen-level air temperature in different LCZ classes of Hong Kong.

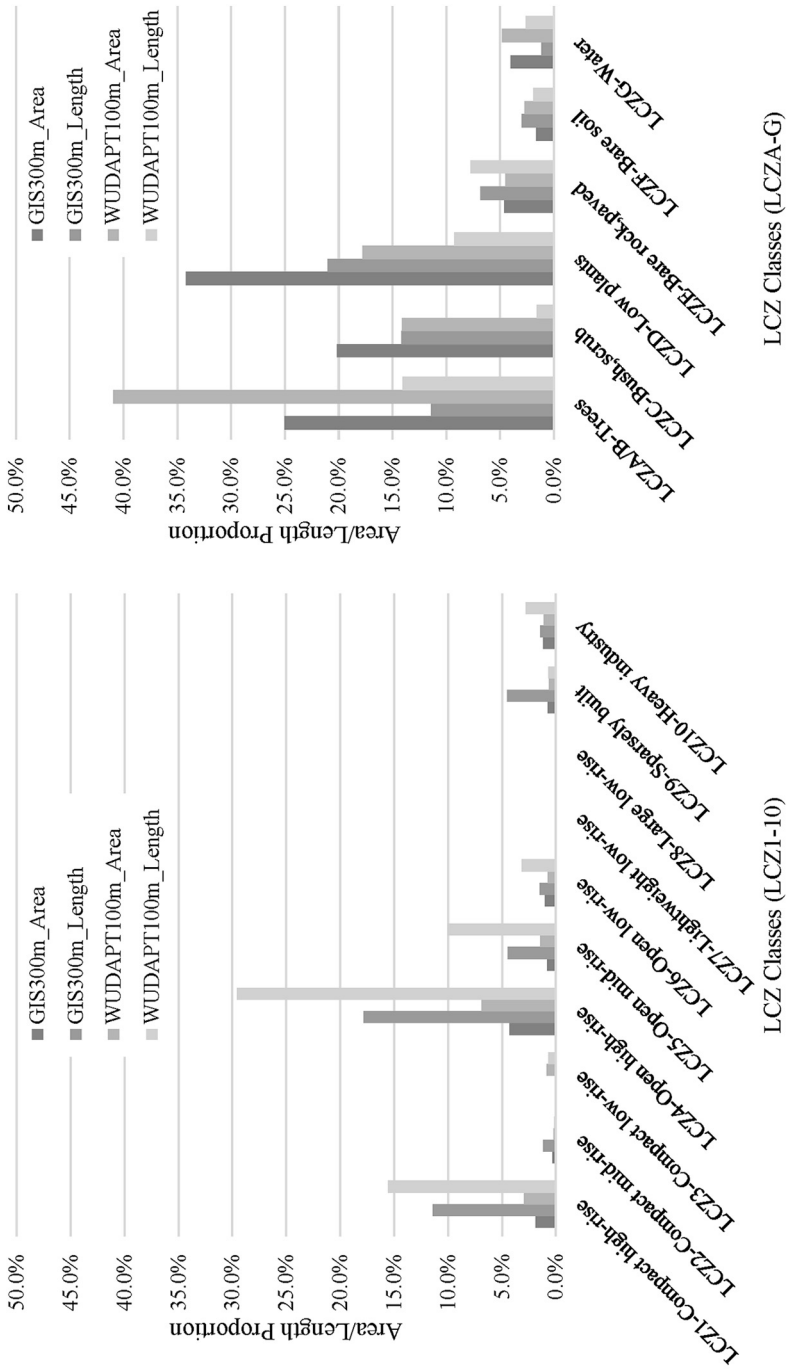

Fig. 4. The areal proportion and corresponding composition of the route length in different LCZ classes.

Table 3
Summary of the meteorological conditions of the days during the mobile measurement. All data shown in this table are based on the weather records of the HKO meteorological stations (The time of sunset and sunrise during the survey dates are approximate 6:00 and 19:00. Run No.12 was a supplemental measurement because there was an instrumental error during the evening run on 27 Oct 2016. As shown in the table, the weather conditions of these two dates were similar).

Run no.	Date	Time period	Routes	Air temp. (T_a, °C)	Relative humidity (RH, %)	Mean wind speed (v, m/s)	Sky condition (Oktas)
1	17-Jul-16	09:00–11:00	Route-1	30.5–31.4	71–77	2.8	3
2	23-Jul-16	14:00–16:00	Route-1	32.1–32.4	64–66	3.8	3
3	23-Jul-16	19:00–21:00	Route-1	30.1–30.4	75–77	0.6	3
4	24-Aug-16	09:00–11:00	Route-1	29.8–31.3	65–70	1.9	4
5	24-Aug-16	14:00–16:00	Route-1	33.0–33.3	60–63	3.5	3
6	24-Aug-16	19:00–21:00	Route-1	29.4–29.9	75–81	3.5	3
7	25-Aug-16	09:00–11:00	Route-1	29.9–31.4	72–78	2.2	4
8	25-Aug-16	14:00–16:00	Route-1	33.9–34.3	63–64	3.4	2
9	25-Aug-16	19:00–21:00	Route-1	30.0–30.4	75–78	1.3	2
10	27-Oct-16	09:00–11:00	Route-2	28.9–29.7	73–81	1.9	5
11	27-Oct-16	14:00–16:00	Route-2	32.6–34.0	59–65	3.0	2
12	15-Aug-17	19:00–21:00	Route-2	29.3–30.0	73–75	1.4	2

filter a suitable method for processing the mobile measurement data with inherent spatial characteristics. A general 1-D median filter is shown as follows:

$$\hat{x}(n) = median[y(n-T),...,y(n-1),y(n),y(n+1),...,y(n+T)] \tag{1}$$

where the median $\hat{x}(n)$ was calculated within a moving window with the size of $W = 2T + 1$. The spikes within the range of the moving window were detected by re-sorting the data in the moving window and the out-of-range values were replaced by the calculated median $\hat{x}(n)$. The moving window W slid along the entire data sequence to eliminate all suspected spikes. To determine an appropriate W for the median filter of the mobile measurement data, all data were imported into GIS for semivariogram ($\hat{\gamma}$) modelling. $\hat{\gamma}$ is defined as a function of distance and shown as the following equation (O'Sullivan and Unwin 2014):

$$\hat{\gamma} = \frac{1}{2n(d)} \sum_{s_i - s_j = d} (T_{ai} - T_{aj})^2 \tag{2}$$

All spatially distributed mobile measurement data points were paired (s_i and s_j). d is the distance between the two points of each pair. T_{ai} and T_{aj} are the observed T_a at s_i and s_j. $n(d)$ is the total number of the pairs of all spatial points. As a function of d, the value of the semivariogram continues to increase until a certain limit [usually defined as a value of 95% of the sill, $\sigma(0)$] at a certain distance of $d = r$. The r can be identified by fitting a semivariogram curve using ordinary least squares (OLS). The number of the data points in a corresponding circular area (with a diameter $= r$) was used as the size W of the moving window in the median filtering of the data sequence. At the end of the above process, the unwanted data spikes caused by the random impacts were removed.

After the above preprocessing, all data were mapped in GIS combined with the GIS- and WUDAPT-based LCZ classification maps for further analysis. The present study concerns two kinds of differences/variations in T_a – differences between different LCZ classes ($\Delta T_{a,\ LCZ\ X-LCZ\ Y}$) and the intra-LCZ variability ($\sigma T_{a,\ LCZ\ X}$). The $\Delta T_{a,\ LCZ\ X-LCZ\ Y}$ is defined as:

$$\Delta T_{a,\ LCZ\ X-LCZ\ Y} = |\overline{T_{a,LCZ\ X}} - \overline{T_{a,LCZ\ Y}}| \tag{3}$$

where $\Delta T_{a,\ LCZ\ X-LCZ\ Y}$ is the absolute difference of averaged T_a between LCZ X and LCZ Y. $\overline{T_{a,LCZ\ X}}$ and $\overline{T_{a,LCZ\ Y}}$ are the mean of the measured T_a in LCZ X and LCZ Y respectively. The $T_{a,\ LCZ\ X}$ is defined as:

$$\overline{T_{a,LCZ\ X}} = \frac{1}{n} \sum_{i=1}^{n} T_{a,LCZ\ X_i} \tag{4}$$

where n is the total number of all T_a data points measured in all area of the LCZ X. $T_{a,\ LCZ\ Xi}$ is the measured value of T_a at the location i on the mobile measurement route. The $\sigma T_{a,\ LCZ\ X}$ is defined as:

$$\sigma T_{a,\ LCZ\ X} = \sqrt{\frac{1}{n} \sum_{i=1}^{n} (T_{a,LCZ\ X_i} - \overline{T_{a,LCZ\ X}})^2} \tag{5}$$

where $\sigma T_{a,\ LCZ\ X}$ is the standard deviation of all T_a data points measured in LCZ X. A one-way analysis was performed for the processed T_a dataset mentioned earlier in this section by different LCZ classes. For the data of each LCZ class, the Analysis of Variance (ANOVA) test and Student's t-test were performed to compare the average air temperatures in different LCZ classes ($\overline{T_{a,LCZ\ X}}$, $\overline{T_{a,LCZ\ Y}}$, etc.). The above tests were also used to determine if there is any significant difference in the average air temperatures among LCZ classes (at a significant level of $\alpha = 0.05$).

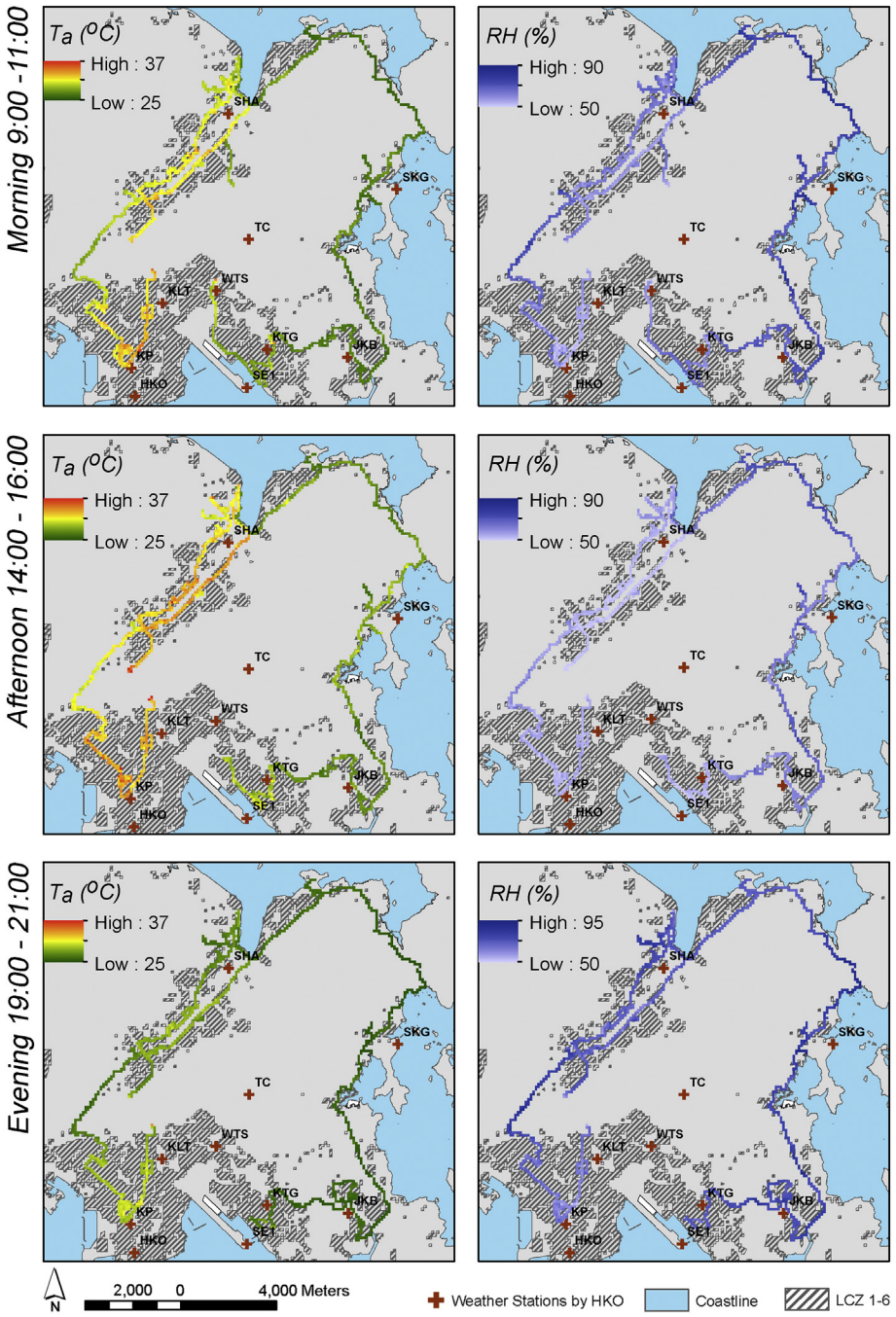

Fig. 5. The spatial variation of measured screen-level T_a and RH along the two measurement routes during daytime and nighttime. (Fig. S1-S3 in the Supplementary material show the enlarged plots of the T_a panels).

3. Results

3.1. Mobile measurement data analysis results

The spatial variation of measured screen-level T_a and *RH* along the two measurement routes during daytime and nighttime is plotted in Fig. 5. There were three time slots. The measurement periods of 9:00–11:00 and 14:00–16:00 were combined to represent daytime conditions; the period of 19:00–21:00 was used to reflect nighttime conditions. A considerable air temperature difference between high-density urban built-up area (LCZs 1 to 6) and other LCZ classes was observed. The highest temperature was observed in the high-density downtown area of Kowloon (mainly LCZ 1, LCZ 4. The bottom left part of the route map, near the HKO and KP

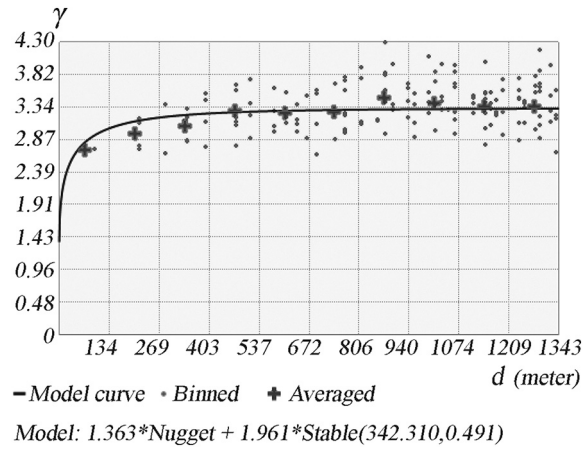

Fig. 6. The resultant semivariogram model and the fitted curve based on the mobile measurement T_a data. The semivariogram reached 95% of the upper limit (the sill, σ(0)) at a distance of 342.31 m.

weather stations). Relatively higher temperatures also appear in the Shatin new town in the New Territories (mainly LCZ4, close to the SHA weather station).

Fig. 6 shows the resultant semivariogram model and fitted curve based on the mobile measurement T_a data. The semivariogram reached 95% of the upper limit (the sill, $\sigma(0)$) at a distance of approximately 340 m. Therefore, this spatial scale was identified as an appropriate spatial scale to calculate the size of the moving window for the median filtering. The size of the moving window was determined to be 30 (because it takes an average of approximately 30s to pass through a distance of 340 m during the mobile measurement campaigns).

3.2. Air temperature difference and LCZ classifications

3.2.1. Variation in air temperature among different LCZ classes

One-way analysis was performed for the T_a data by different LCZ classes based on both the 300 m-resolution GIS-based LCZ map (Fig. 7) and the 100 m-resolution WUDAPT map (Fig. 8) of Hong Kong. Both daytime and the nighttime T_a data were analyzed. For the data of each LCZ class, an Analysis of Variance (ANOVA) test was performed to calculate the $\overline{T_{a,LCZ\ X}}$. The Student's *t*-test was performed to compare the $\overline{T_{a,LCZ\ X}}$ of different LCZ classes (at a significant level of $\alpha = 0.05$).

A significant difference can be found in the air temperature between built-up classes (LCZ 1 to LCZ 10) and land cover classes (LCZ A to LCZ G) for both the GIS LCZ map and the WUDAPT map. It implies that both versions of LCZ classifications can well represent the urban-rural contrast in screen-level air temperature. The Student's *t*-test results show that there are significant T_a differences between most of the built-up classes (LCZ 1 to LCZ 10), which indicates that both versions of LCZ classification maps have successfully depicted the intra-urban air temperature difference (in the built-up area). In Hong Kong, the densely populated areas largely consist of six built-up classes, from LCZ 1 to LCZ 6 (labelled in Fig. 3). Therefore, the present study paid more attention to these six classes due to their relevance to urban living. The ordered difference reports were prepared using the Student's t-test for the daytime and nighttime air temperature differences based on two versions of the LCZ classification maps. As a result, the $\Delta T_{a,\ LCZ\ X-LCZ\ Y}$ of each pair of LCZs 1 to 6 was calculated and shown in Fig. 9 and Fig. 10.

By comparing the above results of LCZ 1 to LCZ 6 (Table 4), some common findings about air temperature differences can be summed up:

(1) LCZ 1 compact high-rise area has the highest air temperature during nighttime. It is approximately 0.9 °C higher than the LCZ 2 compact mid-rise area and 0.5–1.1 °C higher than the LCZ 4 open high-rise area. This result is similar to other cities and within our expectation. The compactly arranged buildings in LCZ 1 slow down the night heat dissipation process.

(2) During daytime, the T_a differences between LCZ 1, LCZ 2, and LCZ 3 are commonly smaller than those during nighttime. The GIS-based results show that the pattern of $\overline{T_{a,LCZ\ 1}} > \overline{T_{a,LCZ\ 2}} > \overline{T_{a,LCZ\ 3}}$ remains unchanged across the day.

(3) $\Delta T_{a,\ LCZ\ 2-LCZ\ 4}$ and $\Delta T_{a,\ LCZ\ 2-LCZ\ 5}$ are relatively small, indicating that besides the urban morphological indicators used in the LCZ classification system, there are other underlying variables that have an influence on the screen-level air temperature in the complex geographic setting of Hong Kong. These underlying influential variables include but are not limited to relief, terrain, proximity to water bodies, rural soil moisture, sea breeze, unevenly distributed anthropogenic heat sources, and highly heterogeneous vegetation species, etc.

(4) The GIS-based results also indicate that $\overline{T_{a,LCZ\ 6}}$ and $\overline{T_{a,LCZ\ 5}}$ are higher than $\overline{T_{a,LCZ\ 4}}$ and $\overline{T_{a,LCZ\ 1}}$ during daytime. During daytime, the total incoming solar radiation in LCZ 5 and LCZ 6 is much larger than LCZ 1 and LCZ 4 because of less shading. Similarly, relatively high daytime air temperature is also observed in other cases (Quanz et al. 2018, Skarbit et al. 2017). It should be noted that, the situation could vary between different cities. It is highly dependent on their individual latitudes (which can affect the

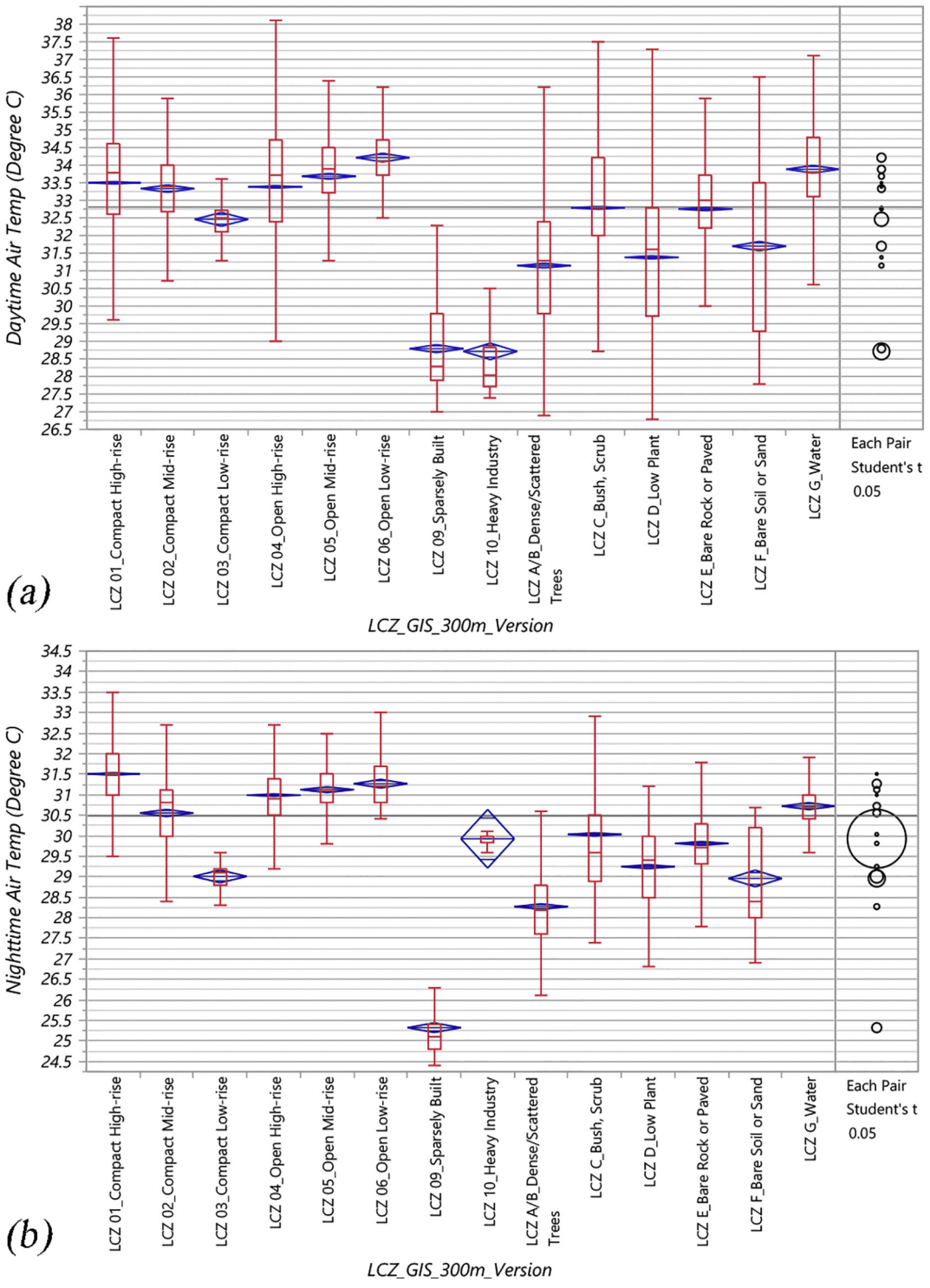

Fig. 7. The one-way analysis result of the daytime (a) and nighttime air temperature (b) by the 300 m-resolution GIS-based LCZ classification map.

amount of incoming solar radiation) and climate types (which can lead to different levels of the temperature variation between day and night), etc. The above further confirms the significance of shadings in the improvement of screen-level thermal environment under the meteorological condition of subtropical cities, such as Hong Kong.

However, the pattern of $\overline{T_{a,LCZ\ 6}}$ / $\overline{T_{a,LCZ\ 5}}$ > $\overline{T_{a,LCZ\ 4}}$ / $\overline{T_{a,LCZ\ 1}}$ does not appear in the WUDAPT-based results. It can be attributed to

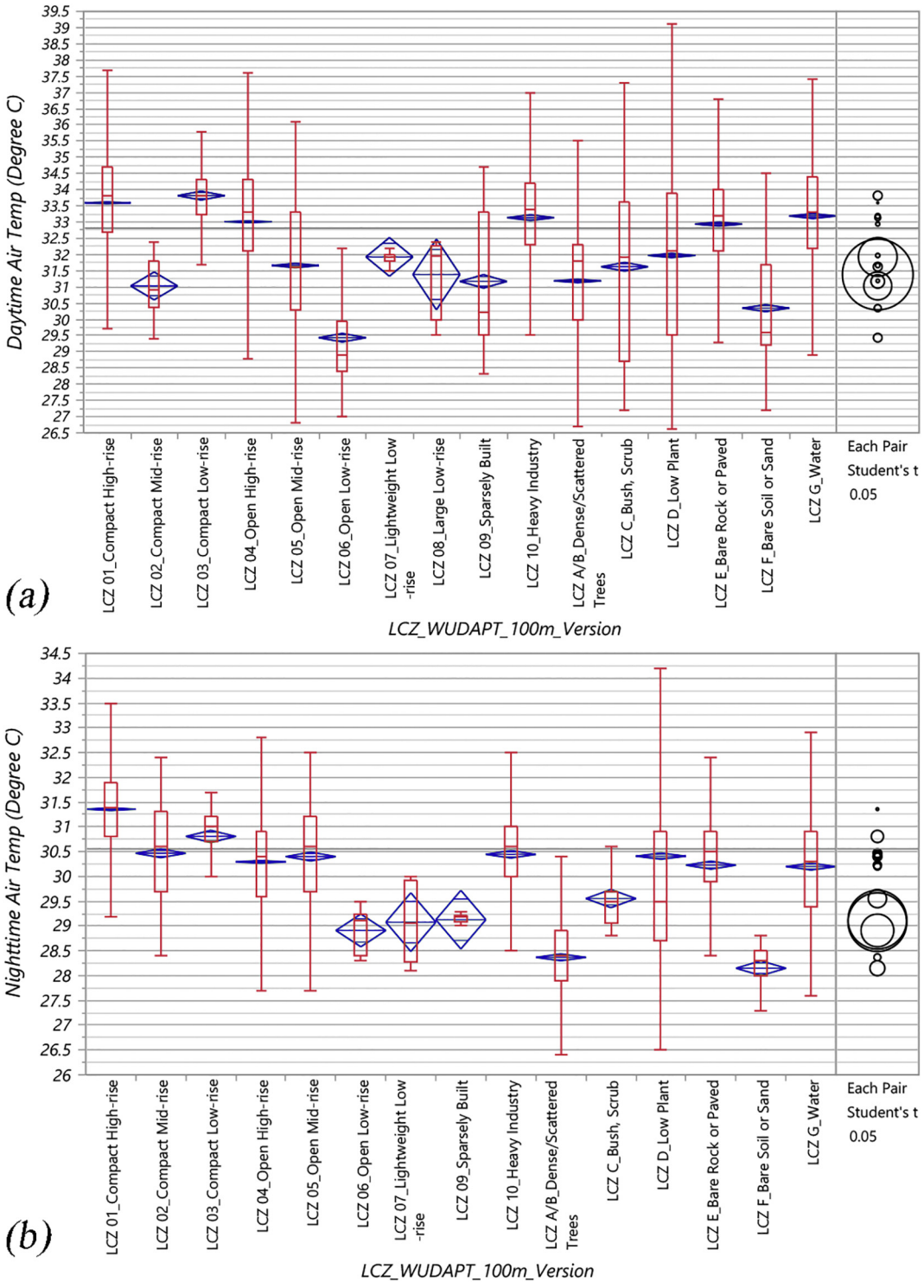

Fig. 8. The one-way analysis result of the daytime (a) and nighttime air temperature (b) by the 100 m-resolution WUDAPT method LCZ classification map.

the fundamental difference between the two classification methods. The GIS-based method largely depends on real morphological features while the WUDAPT method is a workflow basing entirely on Landsat imagery and random forest classification scheme (Mills et al. 2015). In the WUDAPT method, radiation could be a significant factor because it affects the remote sensing signal in different spectral bands of the satellite images. Significant differences have been observed between GIS and WUDAPT results in the T_a of LCZ 6

Ordered Differences Report Comparisons for each pair using Student's t

Daytime Air Temperature (℃) / GIS-300m

Level	- Level	Difference	Std Err Dif	Lower CL	Upper CL	p-Value
LCZ 06_Open Low-rise	LCZ 03_Compact Low-rise	1.75	0.116	1.53	1.98	<.0001 *
LCZ 05_Open Mid-rise	LCZ 03_Compact Low-rise	1.22	0.105	1.02	1.43	<.0001 *
LCZ 01_Compact High-rise	LCZ 03_Compact Low-rise	1.04	0.099	0.84	1.23	<.0001 *
LCZ 04_Open High-rise	LCZ 03_Compact Low-rise	0.92	0.099	0.73	1.12	<.0001 *
LCZ 06_Open Low-rise	LCZ 02_Compact Mid-rise	0.88	0.081	0.72	1.04	<.0001 *
LCZ 02_Compact Mid-rise	LCZ 03_Compact Low-rise	0.87	0.111	0.66	1.09	<.0001 *
LCZ 06_Open Low-rise	LCZ 04_Open High-rise	0.83	0.064	0.70	0.95	<.0001 *
LCZ 06_Open Low-rise	LCZ 01_Compact High-rise	0.71	0.064	0.59	0.84	<.0001 *
LCZ 06_Open Low-rise	LCZ 05_Open Mid-rise	0.53	0.074	0.38	0.67	<.0001 *
LCZ 05_Open Mid-rise	LCZ 02_Compact Mid-rise	0.35	0.066	0.22	0.48	<.0001 *
LCZ 05_Open Mid-rise	LCZ 04_Open High-rise	0.30	0.043	0.22	0.38	<.0001 *
LCZ 05_Open Mid-rise	LCZ 01_Compact High-rise	0.18	0.043	0.10	0.27	<.0001 *
LCZ 01_Compact High-rise	LCZ 02_Compact Mid-rise	0.17	0.054	0.06	0.27	0.0023 *
LCZ 01_Compact High-rise	LCZ 04_Open High-rise	0.12	0.022	0.07	0.16	<.0001 *
LCZ 04_Open High-rise	LCZ 02_Compact Mid-rise	0.05	0.055	-0.06	0.16	0.3641

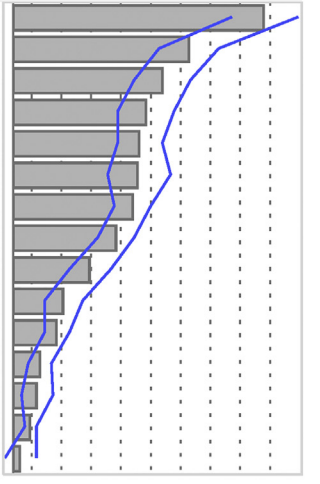

Nighttime Air Temperature (℃) / GIS-300m

Level	- Level	Difference	Std Err Dif	Lower CL	Upper CL	p-Value
LCZ 01_Compact High-rise	LCZ 03_Compact Low-rise	2.50	0.062	2.38	2.62	<.0001 *
LCZ 06_Open Low-rise	LCZ 03_Compact Low-rise	2.26	0.073	2.11	2.40	<.0001 *
LCZ 05_Open Mid-rise	LCZ 03_Compact Low-rise	2.11	0.067	1.98	2.24	<.0001 *
LCZ 04_Open High-rise	LCZ 03_Compact Low-rise	1.98	0.062	1.86	2.10	<.0001 *
LCZ 02_Compact Mid-rise	LCZ 03_Compact Low-rise	1.54	0.069	1.41	1.68	<.0001 *
LCZ 01_Compact High-rise	LCZ 02_Compact Mid-rise	0.95	0.036	0.88	1.02	<.0001 *
LCZ 06_Open Low-rise	LCZ 02_Compact Mid-rise	0.71	0.053	0.61	0.82	<.0001 *
LCZ 05_Open Mid-rise	LCZ 02_Compact Mid-rise	0.57	0.043	0.48	0.65	<.0001 *
LCZ 01_Compact High-rise	LCZ 04_Open High-rise	0.52	0.016	0.49	0.55	<.0001 *
LCZ 04_Open High-rise	LCZ 02_Compact Mid-rise	0.44	0.035	0.37	0.50	<.0001 *
LCZ 01_Compact High-rise	LCZ 05_Open Mid-rise	0.38	0.030	0.33	0.44	<.0001 *
LCZ 06_Open Low-rise	LCZ 04_Open High-rise	0.28	0.042	0.20	0.36	<.0001 *
LCZ 01_Compact High-rise	LCZ 06_Open Low-rise	0.24	0.042	0.15	0.32	<.0001 *
LCZ 06_Open Low-rise	LCZ 05_Open Mid-rise	0.15	0.049	0.05	0.24	0.0032 *
LCZ 05_Open Mid-rise	LCZ 04_Open High-rise	0.13	0.030	0.08	0.19	<.0001 *

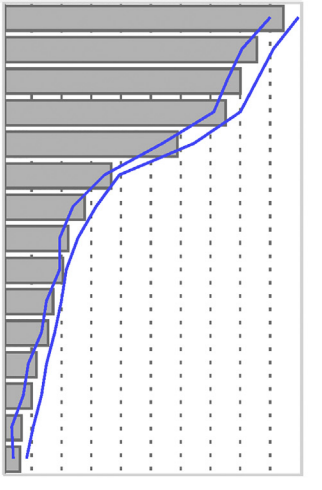

Fig. 9. The ordered difference reports of the daytime and nighttime air temperature by the 300 m-resolution GIS-based LCZ classification.

Ordered Differences Report **Comparisons for each pair using Student's t**

Daytime Air Temperature (℃) / WUDAPT-100m

Level	- Level	Difference	Std Err Dif	Lower CL	Upper CL	p-Value
LCZ 03_Compact Low-rise	LCZ 06_Open Low-rise	4.38	0.094	4.20	4.57	<.0001 *
LCZ 01_Compact High-rise	LCZ 06_Open Low-rise	4.16	0.067	4.03	4.29	<.0001 *
LCZ 04_Open High-rise	LCZ 06_Open Low-rise	3.58	0.067	3.45	3.71	<.0001 *
LCZ 03_Compact Low-rise	LCZ 02_Compact Mid-rise	2.79	0.225	2.35	3.23	<.0001 *
LCZ 01_Compact High-rise	LCZ 02_Compact Mid-rise	2.56	0.214	2.14	2.98	<.0001 *
LCZ 05_Open Mid-rise	LCZ 06_Open Low-rise	2.23	0.074	2.08	2.37	<.0001 *
LCZ 03_Compact Low-rise	LCZ 05_Open Mid-rise	2.16	0.076	2.01	2.31	<.0001 *
LCZ 04_Open High-rise	LCZ 02_Compact Mid-rise	1.98	0.214	1.56	2.40	<.0001 *
LCZ 01_Compact High-rise	LCZ 05_Open Mid-rise	1.93	0.036	1.86	2.00	<.0001 *
LCZ 02_Compact Mid-rise	LCZ 06_Open Low-rise	1.60	0.224	1.16	2.04	<.0001 *
LCZ 04_Open High-rise	LCZ 05_Open Mid-rise	1.35	0.036	1.28	1.42	<.0001 *
LCZ 03_Compact Low-rise	LCZ 04_Open High-rise	0.81	0.069	0.67	0.94	<.0001 *
LCZ 05_Open Mid-rise	LCZ 02_Compact Mid-rise	0.63	0.217	0.21	1.06	0.0036 *
LCZ 01_Compact High-rise	LCZ 04_Open High-rise	0.58	0.019	0.55	0.62	<.0001 *
LCZ 03_Compact Low-rise	LCZ 01_Compact High-rise	0.22	0.069	0.09	0.36	0.0012 *

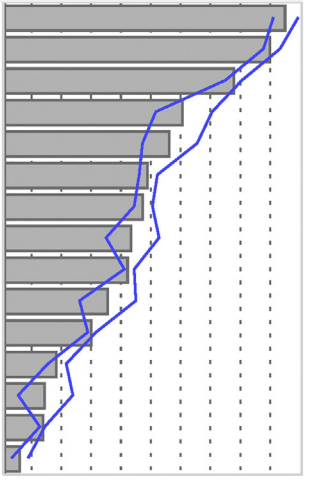

Nighttime Air Temperature (℃) / WUDAPT-100m

Level	- Level	Difference	Std Err Dif	Lower CL	Upper CL	p-Value
LCZ 01_Compact High-rise	LCZ 06_Open Low-rise	2.45	0.142	2.17	2.72	<.0001 *
LCZ 03_Compact Low-rise	LCZ 06_Open Low-rise	1.90	0.151	1.60	2.19	<.0001 *
LCZ 02_Compact Mid-rise	LCZ 06_Open Low-rise	1.56	0.147	1.27	1.84	<.0001 *
LCZ 05_Open Mid-rise	LCZ 06_Open Low-rise	1.49	0.147	1.20	1.78	<.0001 *
LCZ 04_Open High-rise	LCZ 06_Open Low-rise	1.38	0.142	1.10	1.66	<.0001 *
LCZ 01_Compact High-rise	LCZ 04_Open High-rise	1.06	0.016	1.03	1.09	<.0001 *
LCZ 01_Compact High-rise	LCZ 05_Open Mid-rise	0.96	0.040	0.88	1.03	<.0001 *
LCZ 01_Compact High-rise	LCZ 02_Compact Mid-rise	0.89	0.039	0.81	0.97	<.0001 *
LCZ 01_Compact High-rise	LCZ 03_Compact Low-rise	0.55	0.054	0.44	0.66	<.0001 *
LCZ 03_Compact Low-rise	LCZ 04_Open High-rise	0.51	0.054	0.41	0.62	<.0001 *
LCZ 03_Compact Low-rise	LCZ 05_Open Mid-rise	0.41	0.065	0.28	0.53	<.0001 *
LCZ 03_Compact Low-rise	LCZ 02_Compact Mid-rise	0.34	0.065	0.21	0.47	<.0001 *
LCZ 02_Compact Mid-rise	LCZ 04_Open High-rise	0.17	0.039	0.10	0.25	<.0001 *
LCZ 05_Open Mid-rise	LCZ 04_Open High-rise	0.11	0.040	0.03	0.19	0.0074 *
LCZ 02_Compact Mid-rise	LCZ 05_Open Mid-rise	0.07	0.054	-0.04	0.17	0.2190

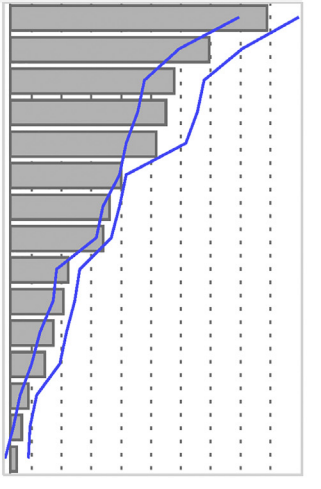

Fig. 10. The ordered difference reports of the daytime and nighttime air temperature by the 100 m-resolution WUDAPT method LCZ classification.

Table 4
Summary of the pattern of air temperature differences among LCZs 1 to 6 based on the GIS-300 m and WUDAPT-100 m versions of the LCZ classification map of Hong Kong.

LCZ classification	Daytime/nighttime	Summary of the pattern of air temperature differences among LCZs 1 to 6 [a]
GIS-300 m	Daytime	$\overline{T_{a,LCZ\ 6}} > \overline{T_{a,LCZ\ 5}} > \overline{T_{a,LCZ\ 1}} > \overline{T_{a,LCZ\ 4}} \approx \overline{T_{a,LCZ\ 2}} > \overline{T_{a,LCZ\ 3}}$
GIS-300 m	Nighttime	$\overline{T_{a,LCZ\ 1}} > \overline{T_{a,LCZ\ 6}} > \overline{T_{a,LCZ\ 5}} > \overline{T_{a,LCZ\ 4}} > \overline{T_{a,LCZ\ 2}} > \overline{T_{a,LCZ\ 3}}$
WUDAPT-100 m	Daytime	$\overline{T_{a,LCZ\ 3}} > \overline{T_{a,LCZ\ 1}} > \overline{T_{a,LCZ\ 4}} > \overline{T_{a,LCZ\ 5}} > \overline{T_{a,LCZ\ 2}} > \overline{T_{a,LCZ\ 6}}$
WUDAPT-100 m	Nighttime	$\overline{T_{a,LCZ\ 1}} > \overline{T_{a,LCZ\ 3}} > \overline{T_{a,LCZ\ 2}} \approx \overline{T_{a,LCZ\ 5}} > \overline{T_{a,LCZ\ 4}} > \overline{T_{a,LCZ\ 6}}$

[a] $\overline{T_{a,LCZ\ X}} > \overline{T_{a,LCZ\ Y}}$ indicates that the air temperature in LCZ X is significantly different from LCZ Y (higher). $\overline{T_{a,LCZ\ X}} \approx \overline{T_{a,LCZ\ Y}}$ indicates that no statistically significant air temperature difference was found between LCZ X and LCZ Y.

in both daytime and nighttime. The T_a of WUDAPT LCZ 6 is much lower than GIS LCZ 6 because many sparsely-built villages (LCZ 9 sites in the GIS-based LCZ map) with a low T_a in the coastal area of Sai Kung were mistaken as LCZ 6 by the WUDAPT classification. There are also noticeable differences in the nighttime T_a of LCZ 3 because many open low-rise areas (LCZ 6 sites in the GIS-based LCZ map) were identified as the LCZ 3 by the WUDAPT classification. The above observation implies that the criteria for the determination of the compactness of low-rise areas should be further refined in WUDAPT. In other words, it is important to differentiate between "compact" and "open" more accurately. The pattern of T_a in LCZ7 - LCZ9 is not stable because the areas of these LCZ classes are extremely small in Hong Kong (as mentioned earlier in Section 2.2.1).

3.2.2. Intra-LCZ variability

The $\sigma T_{a,\ LCZ\ X}$ of each LCZ class was calculated (Table 5). The results show that all daytime $\sigma T_{a,\ LCZ\ X}$ are approximately two times larger than nighttime, because of the influence of solar radiation. To be more specific, even in a high-density urban context with a homogeneous morphological form, the incoming shortwave solar radiation is still unevenly distributed at different locations due to the complicated shading of the densely constructed building clusters. It further leads to considerable spatial variability in screen-level air temperatures. The above spatial variabilities have been observed in the urban context of Hong Kong in a previous study (Shi et al. 2015). In that study, the spatial distribution of daytime screen-level air temperature was separately measured in the two study areas of Tsim Sha Tsui, Kowloon (mainly LCZ 1) and Tai Po, New Territories (LCZ 5 and LCZ 2). A range (measured as the $T_{a,\ max,\ LCZ\ X} - T_{a,\ min,\ LCZ\ X}$) of up to 2 °C was measured in both study areas (Fig. 11). Moreover, the pattern of $\sigma T_{a,\ LCZ\ 1} > \sigma T_{a,\ LCZ\ 2} > \sigma T_{a,\ LCZ\ 3}$ does not change across daytime and nighttime, which further proves the influence of the shading effect of high-rise buildings on the intra-LCZ variability of screen-level air temperature.

By comparing the $\sigma T_{a,\ LCZ\ X}$ (LCZ 1 to LCZ 6) calculated based on the two different versions of LCZ classification maps, it was found that the GIS-300 m version of LCZ classification map produced a much smaller $\sigma T_{a,\ LCZ\ 3}$, $\sigma T_{a,\ LCZ\ 6}$ than the WUDAPT-100 m version (almost 50% smaller). The smaller $\sigma T_{a,\ LCZ\ X}$ in low-rise building areas indicates that the GIS-based LCZ classification method provides a more accurate classification for these areas than WUDAPT. The reason is that the GIS-based method involves a large amount of precise building data from surveying. Such data are not used in the current WUDAPT method. However, it was also found that both the GIS-300 m and WUDAPT-100 m LCZ classification maps produce a relatively large $\sigma T_{a,\ LCZ\ 1}$, $\sigma T_{a,\ LCZ\ 4}$ of 1.8–2.0 °C and a $\sigma T_{a,\ LCZ\ 2}$, $\sigma T_{a,\ LCZ\ 5}$ of 1.3–2.0 °C. The above $\sigma T_{a,\ LCZ\ X}$ is already larger than many of the $\Delta T_{a,\ LCZ\ X-LCZ\ Y}$ (refers to the Fig. 9 and Fig. 10). The results of $\sigma T_{a,\ LCZ\ X} > \Delta T_{a,\ LCZ\ X-LCZ\ Y}$ reveal that there are still other influential variables of screen-level air temperature that are not being considered in the current two versions of LCZ classification maps of Hong Kong (as indicated, for example, the unevenly distributed anthropogenic heat sources, heterogeneous vegetation species, and influence of incoming solar radiation). It has been clearly identified that the dominant microclimate impact factors are different across LCZ sites (Shi et al. 2015). Taking the two LCZ sample sites shown in Fig. 11 as an example, we identified that the dominant effect of air temperature in the Tsim Sha Tsui site (LCZ 1) was building morphology (measured as SVF). In contrast, urban greening and the surrounding vegetated mountainous topography were more influential in the air temperature in the Tai Po site (LCZ 2 and LCZ 5). Therefore, the effects of complex terrain, relief, water bodies, soil moisture, etc. are also parts of the influencing factors of the observed intra-LCZ variability of air temperature of Hong Kong. A similar micro-scale variability of air temperature was also observed in other cases (Quanz et al.

Table 5
Summary of the intra-LCZ variability of air temperature ($\sigma T_{a,\ LCZ\ X}$, °C) in LCZ 1 to LCZ 6 based on the GIS-300 m and WUDAPT-100 m versions of the LCZ classification map of Hong Kong.

LCZ Class (LCZ 1 to LCZ 6)	Indicator (°C)	GIS-300 m version		WUDAPT-100 m version	
		Daytime	Nighttime	Daytime	Nighttime
LCZ 01 Compact High-rise	$\sigma T_{a,\ LCZ\ 1}$	1.89	0.79	1.74	0.90
LCZ 02 Compact Mid-rise	$\sigma T_{a,\ LCZ\ 2}$	1.31	0.88	0.82	1.00
LCZ 03 Compact Low-rise	$\sigma T_{a,\ LCZ\ 3}$	0.66	0.31	1.19	0.66
LCZ 04 Open High-rise	$\sigma T_{a,\ LCZ\ 4}$	1.97	0.81	2.02	1.00
LCZ 05 Open Mid-rise	$\sigma T_{a,\ LCZ\ 5}$	1.45	0.61	2.05	1.06
LCZ 06 Open Low-rise	$\sigma T_{a,\ LCZ\ 6}$	0.75	0.49	1.49	0.41

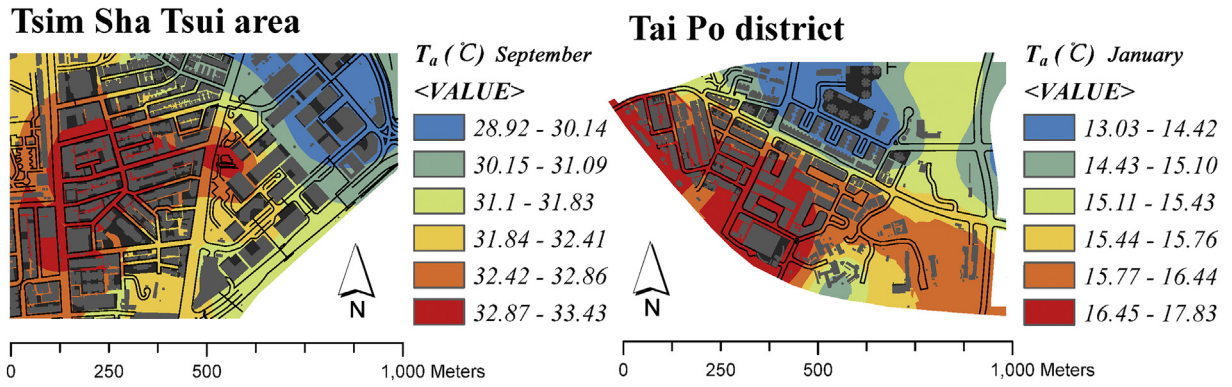

Fig. 11. The daytime screen-level air temperature in the two study areas respectively. Modified from Shi et al. (2015).

2018). They need to be taken into consideration in further LCZ/WUDAPT urban climate research.

3.2.3. Influencing building morphological factors of air temperature

It has been found that building morphology has a considerable influence on the intraurban spatial variability of air temperature, especially in the high-density urban context of Hong Kong (Shi, Katzschner, and Ng 2018). In the present study, a multivariate analysis was performed in order to identify the most important building morphological factors of the intraurban variability of air temperature. To be more specific, a series of correlation analysis between the site-averaged daytime/nighttime air temperature and the three building morphological factors - λ_b, Z_h, Ψ_{svf} (adopted in the LCZ classification process of this study; Section 2.2.1) were conducted. The results (Table 6) show that both the Z_h and Ψ_{svf} have a significant correlation with site averaged temperature. The influence of building morphology on air temperature is even stronger during nighttime. The influence of Ψ_{svf} on the urban air temperature differences has been indicated by local researchers (Chen et al. 2012), and further validated by the LCZ scheme and mobile measurement data in this study.

4. Discussion and conclusions

4.1. GIS-based method and WUDAPT method of LCZ classification in the high-density urban scenario

The LCZ classification mapping study of Hong Kong is one of the first applications of the LCZ system in such an extremely compact and high-density urban scenario under the subtropical climatic condition. It has been reported by some researchers that the LCZ scheme is not always suitable for the Asian cities due to their unique urban contexts and the combination of land-use and building morphology. They commented that the criteria should be slightly modified to adapt to the local context (Kotharkar and Bagade 2017). However, the above concern does not seem to materialize in the present study. Although the built-up areas of Hong Kong are extremely dense, the standard morphological values of LCZ classes proposed by Stewart and Oke (2012) were strictly followed during the classification process. In the present study, no modification was made to the classification criteria. However, there are still certain advantages and disadvantages of using the two LCZ mapping methods. Table 7 provides a brief discussion about the limitation and potential of the two methods for future urban climate studies. It could be expected that a combination of both methods would provide a more robust and accurate LCZ classification/map for further urban climatic research.

4.2. Evaluating the current LCZ/WUDAPT mappings of Hong Kong by mobile measurement

The current LCZ/WUDAPT mappings in Hong Kong were evaluated by mobile measurement campaigns. Significant variations in air temperature between different LCZ classes were observed. In the present study, the mobile measurement campaigns have overcome the monitoring gaps of sparsely distributed fixed weather stations and provide more comprehensive spatial information of screen-level air temperature at a finer spatial scale. By investigating the actual measured data from the mobile measurement, this study illustrates that both the urban-rural contrast and differences in screen-level air temperature between LCZ classes can be appropriately depicted for Hong Kong by using the current LCZ maps (both the GIS-300 m and WUDAPT-100 m versions). The study results evaluate the usefulness of the LCZ classification mapping for Hong Kong in delivering reliable data to urban climate

Table 6
The Pearson Correlation Coefficient (R) between the LCZ site-averaged air temperature and building morphological parameters.

	Building surface fraction (λ_b)	Building height (Z_h)	Sky view factor (Ψ_{svf})
Daytime air temperature ($T_{a,\ daytime}$)	0.14	0.34	−0.33
Nighttime air temperature ($T_{a,\ nighttime}$)	0.33	0.48	−0.47

Table 7
A brief summary of the advantages and disadvantages of GIS-based and WUDAPT method for LCZ classification mapping in high-density urban scenario.

	GIS-based Method	WUDAPT Method
Input data requirement	This method has a high requirement for the input datasets. It requires comprehensive and high-quality urban land use and building surveying datasets from local authorities, which might not always be available.	All required data, software and generated results of WUDAPT are free and can be publicly accessed. It makes this method work well with the lack of precise urban morphology data. The feasibility of this method is high.
Classification Criteria/ Procedure	Different cities may have different classification criteria/ procedures, depending on their own reality of urban scenario and data availability. In some cases, the original LCZ scheme has to be slightly modified/adjusted based on the local context in order to avoid "unclassified areas".	The WUDAPT method strictly follows a standardized working procedure for data collection and data processing. The method takes the advantages of machine-learning and remote-sensing technology. The whole working procedure ensures a high working efficiency and makes the automation process possible.
Spatial resolution of outputs	The spatial resolution of the resultant GIS-based LCZ maps usually ranges from 200 m to 500 m depending on the local context/situations. Sensitivity tests are usually required to determine a suitable resultant spatial resolution. The spatial resolution of 200–500 m for the GIS method is a suitable scale for local climate studies.	A unified global standard spatial resolution – 100 m was used, which could be a big advantage in the integration/collation of the LCZ data from different cities/regions. It is also an ideal data platform for intercity cross comparison studies and other worldwide collaboration research.
The accuracy of the classification results	High accuracy could be expected because the method takes full advantages of the accurate, comprehensive and detailed urban datasets from local authorities. The standard values proposed by the LCZ scheme and the application of GIS produce more objective and robust results. At the district level, the GIS-based method detects more urban form details than the WUDAPT method. The GIS results are more detailed/accurate than the WUDAPT results in investigating urban built-up areas (LCZs 1 to 6).	The accuracy of the resultant classification highly depends on the selection of training samples. The subjective artificial visual interpretation method may introduce certain biases/ errors to the classification results. Well-trained experts with a good understanding of local urban context must be involved to ensure the classification accuracy. However, the WUDAPT method classifies land cover types more accurately because it employs remote-sensing technology.
Potential applications	Urban planning/design optimization; Site selection for UHI and microscale urban climate/thermal comfort studies. Etc.	Enhanced Input dataset for improving the mesoscale and region scale weather forecast and climatic modelling. Etc.

researchers as well as local planners and architects. By classifying the urban morphological variables, land use, and surface properties that directly influence the spatial variability of screen-level air temperature (such as building height, ground coverage ratio, sky view factors, and the fraction of vegetation), the two current LCZ maps are readily applicable for further local urban climate research.

4.3. Limitations

The effects of atmospheric mixing could vary under different synoptic types. There are only a limited number of the measurements in the present study, and more measurement campaigns should be conducted to cover different weather/synoptic types of Hong Kong. In addition, it needs to be recognized that the effects of complex terrain, relief, water bodies, soil moisture, etc. are also parts of the influencing factors of the observed inter- and intra-LCZ variability of air temperature of Hong Kong. However, the heterogeneous and complex geography of Hong Kong means that the above effects vary from site to site. Hence, they are difficult to be fully investigated in one single study. Further investigations need to be conducted by selecting locally representative sites within the LCZ classes such as what has been done by Bokwa et al. (2015). Last but not the least, the current study still focusses on the LCZ/WUDAPT mapping. Therefore, the priority was given to the spatial coverage of the measurement data. In order to improve the representativeness of the data, follow-up work should also focus on improving the mobile measurement and data extraction methods.

4.4. Future work - dealing with the intra-LCZ variability

The intra-LCZ variability caused by the high-density heterogeneous urban environment was observed by this study, especially in LCZ 1 to LCZ 6. It implies that further refinement of the classification method/mapping procedure is necessary to improve the classification accuracy for both the GIS-based and WUDAPT methods. Bokwa et al. (2015) have conducted an in-depth study on the investigation of the influence of relief on the urban air temperature. Similar investigations are highly necessary in Hong Kong. In the future, WUDAPT level 1 & 2 data should be considered, since they can provide complete coverage of the urban landscape and include information of individual building elements and features (Xu et al. 2017).

Intra-LCZ variability is also important to urban planning and design because environmental diversity is an important element in improving the environmental quality of urban areas. A diverse urban environment provides a wide range of thermal environments that accommodate different needs of urban dwellers (Lau, Lindberg, et al. 2015a, b). It also allows for a wider choice of planning measures to mitigate the heat island effect. Therefore, future work should focus on the interpretation of the classification maps based on the underlying influential variables of screen-level air temperature mentioned above. Further adjustments and refinements based on the unique local situation/context could provide better information/reference for future urban climate studies. Considering the aforementioned limitations of the present study, future work should also focus on the improvement of the mobile measurement method and extraction of reliable and representative temperature data.

Acknowledgement

This research is supported by the General Research Fund (GRF Project No.: 14643816 and 14629516) from the Research Grants Council (RGC) of Hong Kong. The authors deeply thank the reviewers for their insightful comments, feedbacks and constructive suggestions, recommendations on our research work. The authors also want to appreciate editors for their patient and meticulous work for our manuscript. The authors also thank Ms. Ada Lee of the Chinese University of Hong Kong for her kind help on this paper.

Appendix A. Supplementary data

Supplementary data to this article can be found online at https://doi.org/10.1016/j.uclim.2018.07.001.

References

Alexander, Paul, Mills, Gerald, 2014. Local climate classification and Dublin's urban Heat Island. Atmosphere 5 (4), 755.
Bechtel, Benjamin, Alexander, Paul, Böhner, Jürgen, Ching, Jason, Conrad, Olaf, Feddema, Johannes, Mills, Gerald, See, Linda, Stewart, Iain, 2015. Mapping local climate zones for a worldwide database of the form and function of cities. ISPRS Int. J. Geo-Information 4 (1), 199.
Betanzo, Miko, 2007. Pros and cons of high density urban environments. Build, April/May. pp. 39–40.
Blankenstein, Simone, Kuttler, Wilhelm, 2004. Impact of street geometry on downward longwave radiation and air temperature in an urban environment. Meteorol. Z. 13 (5), 373–379. http://dx.doi.org/10.1127/0941-2948/2004/0013-0373.
Bokwa, Anita, Hajto, Monika J., Walawender, Jakub P., Szymanowski, Mariusz, 2015. Influence of diversified relief on the urban heat island in the city of Kraków, Poland. Theor. Appl. Climatol. 122 (1), 365–382. http://dx.doi.org/10.1007/s00704-015-1577-9.
Chan, Emily Ying Yang, Goggins, William B., Kim, Jacqueline Jakyoung, Griffiths, Sian M., 2012. A study of intracity variation of temperature-related mortality and socioeconomic status among the Chinese population in Hong Kong. J. Epidemiol. Community Health 66 (4), 322–327.
Chen, Liang, Ng, Edward, An, Xipo, Ren, Chao, Lee, Max, Wang, Una, He, Zhengjun, 2012. Sky view factor analysis of street canyons and its implications for daytime intra-urban air temperature differentials in high-rise, high-density urban areas of Hong Kong: a GIS-based simulation approach. Int. J. Climatol. 32 (1), 121–136. http://dx.doi.org/10.1002/joc.2243.
Comrie, Andrew C., 2000. Mapping a Wind–Modified Urban Heat Island in Tucson, Arizona (with Comments on Integrating Research and Undergraduate Learning). In: Bulletin of the American Meteorological Society no. 81. 10. pp. 2417–2431. http://dx.doi.org/10.1175/1520-0477(2000)081<2417:mawmuh>2.3.co;2.
Davenport, Alan G., Sue B Grimmond, C., Oke, Tim R., Wieringa, Jon, 2000. Estimating the roughness of cities and sheltered country. Paper read at Proceedings 12th Conference on Applied Climatology, Asheville, NC. American Meteorological Society, Boston.
Eliasson, Ingegärd, 1990. Urban geometry, surface temperature and air temperature. Energy and Buildings 15 (1), 141–145. http://dx.doi.org/10.1016/0378-7788(90)90125-3.
Eliasson, Ingegärd, 2000. The use of climate knowledge in urban planning. Landsc. Urban Plan. 48 (1), 31–44.
Grimmond, S.U.E., 2007. Urbanization and global environmental change: local effects of urban warming. Geogr. J. 173 (1), 83–88. http://dx.doi.org/10.1111/j.1475-4959.2007.232_3.x.
Hedquist, Brent C., Brazel, Anthony J., 2006. Urban, residential, and rural climate comparisons from mobile transects and fixed stations: Phoenix, Arizona. J. Ariz. Nev. Acad. Sci. 38 (2), 77–87. http://dx.doi.org/10.2181/1533-6085(2006)38[77:URARCC]2.0.CO;2.
Huang, T., Yang, G., Tang, G., 1979. A fast two-dimensional median filtering algorithm. IEEE Trans. Acoust. Speech Signal Process. 27 (1), 13–18. http://dx.doi.org/10.1109/TASSP.1979.1163188.
IPCC, 2014. Climate Change 2014–Impacts, Adaptation and Vulnerability: Regional Aspects. Cambridge University Press, Cambridge, United Kingdom and New York, NY, USA.
Jonsson, Per, 2004. Vegetation as an urban climate control in the subtropical city of Gaborone, Botswana. Int. J. Climatol. 24 (10), 1307–1322. http://dx.doi.org/10.1002/joc.1064.
Kotharkar, Rajashree, Bagade, Anurag, 2017. Local climate zone classification for Indian cities: a case study of Nagpur. Urban Climate. http://dx.doi.org/10.1016/j.uclim.2017.03.003.
Kotharkar, Rajashree, Bagade, Anurag, 2018. Evaluating urban heat island in the critical local climate zones of an Indian city. Landsc. Urban Plan. (169), 92–104. http://dx.doi.org/10.1016/j.landurbplan.2017.08.009.
Landsberg, Helmut E., 1981. The Urban Climate. Vol. 28 Academic press, London.
Lau, Kevin Ka-Lun, Lindberg, Fredrik, Rayner, David, Thorsson, Sofia, 2015a. The effect of urban geometry on mean radiant temperature under future climate change: a study of three European cities. Int. J. Biometeorol. 59 (7), 799–814. http://dx.doi.org/10.1007/s00484-014-0898-1.
Lau, Kevin Ka-Lun, Ren, Chao, Shi, Yuan, Zheng, Venessa, Yim, Steve, Lai, Derrick, 2015b. Determining the optimal size of local climate zones for spatial mapping in high-density cities. In: 9th International Conference on Urban Climate jointly with 12th Symposium on the Urban Environment, Toulouse, France. International Association for Urban Climate (IAUC) and American Meteorological Society (AMS).
Leconte, Francois, Bouyer, Julien, Claverie, Rémy, Pétrissans, Mathieu, 2015. Using local climate zone scheme for UHI assessment: evaluation of the method using mobile measurements. Build. Environ. 83, 39–49. http://dx.doi.org/10.1016/j.buildenv.2014.05.005.
Lehnert, Michal, Geletič, Jan, Husák, Jan, Vysoudil, Miroslav, 2015. Urban field classification by "local climate zones" in a medium-sized Central European city: the case of Olomouc (Czech Republic). Theor. Appl. Climatol. 122 (3), 531–541. http://dx.doi.org/10.1007/s00704-014-1309-6.
Liu, Lin, Lin, Yaoyu, Wang, Dan, Liu, Jing, 2016. An improved temporal correction method for mobile measurement of outdoor thermal climates. Theor. Appl. Climatol.(1–12). http://dx.doi.org/10.1007/s00704-016-1769-y.
Loridan, Thomas, Grimmond, C.S.B., 2012. Characterization of energy flux partitioning in urban environments: links with surface seasonal properties. J. Appl. Meteorol. Climatol. 51 (2), 219–241. http://dx.doi.org/10.1175/jamc-d-11-038.1.
Loridan, Thomas, Lindberg, Fredrik, Jorba, Oriol, Kotthaus, Simone, Grossman-Clarke, Susanne, Grimmond, C.S.B., 2013. High resolution simulation of the variability of surface energy balance fluxes across Central London with urban zones for energy partitioning. Bound.-Layer Meteorol. 147 (3), 493–523. http://dx.doi.org/10.1007/s10546-013-9797-y.
Lowry, William P., 1977. Empirical estimation of urban effects on climate: a problem analysis. J. Appl. Meteorol. 16 (2), 129–135. http://dx.doi.org/10.1175/1520-0450(1977)016<0129:eeoueo>2.0.co;2.
Lu, Jun, Li, Chun-die, Yang, Yong-chuan, Zhang, Xin-hui, Jin, Ming, 2012. Quantitative evaluation of urban park cool island factors in mountain city. J. Cent. South Univ. 19 (6), 1657–1662. http://dx.doi.org/10.1007/s11771-012-1189-9.
McMichael, Anthony J., Woodruff, Rosalie E., Hales, Simon, 2006. Climate change and human health: present and future risks. Lancet 367 (9513), 859–869. http://dx.doi.org/10.1016/S0140-6736(06)68079-3.
Mills, Gerald, Ching, J., See, L., Bechtel, B., Foley, M., 2015. An Introduction to the WUDAPT project. In ICUC9 - 9th International Conference on Urban Climate jointly with 12th Symposium on the Urban Environment Toulouse, France. The International Association for Urban Climate (IAUC) and the American Meteorological Society (AMS).
Ng, Edward, Yuan, Chao, Chen, Liang, Ren, Chao, Fung, Jimmy C.H., 2011. Improving the wind environment in high-density cities by understanding urban morphology and surface roughness: a study in Hong Kong. Landsc. Urban Plan. 101 (1), 59–74. http://dx.doi.org/10.1016/j.landurbplan.2011.01.004.

Nichol, Janet E., Fung, Wing Yee, Lam, Ka-se, Wong, Man Sing, 2009. Urban heat island diagnosis using ASTER satellite images and 'in situ' air temperature. Atmos. Res. 94 (2), 276–284. http://dx.doi.org/10.1016/j.atmosres.2009.06.011.
Oke, Tim R., 1981. Canyon geometry and the nocturnal urban heat island: comparison of scale model and field observations. J. Climatol. 1 (3), 237–254.
Oke, T.R., 2004. Instruments and observing methods: Report No. 81: initial guidance to obtain representative meteorological observations at urban sites. In: World Meteorological Organization, WMO/TD (1250). World Meteorological Organization, Geneva.
Oke, T.R., 2006. Towards better scientific communication in urban climate. Theor. Appl. Climatol. 84 (1), 179–190. http://dx.doi.org/10.1007/s00704-005-0153-0.
O'Sullivan, D., Unwin, D., 2014. Geographic Information Analysis. Wiley, New York.
Peppler, A., 1929. Das Auto als Hilfsmittel der meteorologischen Forschung. Das Wetter 46, 305–308.
Peters, Jan, Van Poppel, Martine, Theunis, Jan, 2012. Air quality mapping in urban environments using mobile measurements. In: Sensing a Changing World. Wageningen, The Netherlands.
PlanD, 2015. Land Utilization in Hong Kong. Hong Kong Planning Department 15 May 2015 2015 [cited 28 Oct 2015]. Available from. http://www.pland.gov.hk/pland_en/info_serv/statistic/landu.html.
Quanz, Justus, Ulrich, Susanne, Fenner, Daniel, Holtmann, Achim, Eimermacher, Jonas, 2018. Micro-scale variability of air temperature within a local climate zone in berlin, Germany, during summer. Climate 6 (1), 5.
Ren, Chao, Ng, Edward Yan-yung, Katzschner, Lutz, 2011. Urban climatic map studies: a review. Int. J. Climatol. 31 (15), 2213–2233. http://dx.doi.org/10.1002/joc.2237.
Ren, Chao, Wang, Ran, Cai, Meng, Xu, Yong, Zheng, Yinsheng, Ng, Edward, 2016. The accuracy of LCZ maps generated by the world urban database and access portal tools (WUDAPT) method: A case study of Hong Kong. In: Paper read at 4th Int. Conf. Countermeasure Urban Heat Islands, Singapore.
Rizwan, Ahmed Memon, Dennis, Leung Y.C., Liu, Chunho, 2008. A review on the generation, determination and mitigation of urban Heat Island. J. Environ. Sci. 20 (1), 120–128. http://dx.doi.org/10.1016/s1001-0742(08)60019-4.
See, L., Perger, C., Duerauer, M., Fritz, S., Bechtel, B., Ching, J., Alexander, P., Mills, G., Foley, M., O' Connor, M., Stewart, I., Feddema, J., Masson, V., 2015. Developing a community-based worldwide urban morphology and materials database (WUDAPT) using remote sensing and crowdsourcing for improved urban climate modelling. In: Paper read at 2015 Joint Urban Remote Sensing Event (JURSE), March 30 2015–April 1 2015.
Shi, Yuan, Ren, Chao, Zheng, Yingsheng, Ng, Edward, 2015. Mapping the urban microclimatic spatial distribution in a sub-tropical high-density urban environment. Archit. Sci. Rev. 1–15. http://dx.doi.org/10.1080/00038628.2015.1105195.
Shi, Yuan, Lau, Kevin Ka-Lun, Ng, Edward, 2016. Developing street-level PM2.5 and PM10 land use regression models in high-density Hong Kong with urban morphological factors. Environ. Sci. Technol. 50 (15), 8178–8187. http://dx.doi.org/10.1021/acs.est.6b01807.
Shi, Yuan, Katzschner, Lutz, Ng, Edward, 2018. Modelling the fine-scale spatiotemporal pattern of urban heat island effect using land use regression approach in a megacity. Sci. Total Environ. (618), 891–904. http://dx.doi.org/10.1016/j.scitotenv.2017.08.252.
Siu, L.W., Hart, M.A., 2012. Quantifying urban heat island intensity in Hong Kong SAR, China. Environ. Monit. Assess. http://dx.doi.org/10.1007/s10661-012-2876-6.
Skarbit, Nóra, Stewart, Iain D., Unger, János, Gál, Tamás, 2017. Employing an urban meteorological network to monitor air temperature conditions in the 'local climate zones' of Szeged, Hungary. Int. J. Climatol. 37 (S1), 582–596. http://dx.doi.org/10.1002/joc.5023.
Stewart, I.D., 2011. A systematic review and scientific critique of methodology in modern urban heat island literature. Int. J. Climatol. 31 (2), 200–217. http://dx.doi.org/10.1002/joc.2141.
Stewart, I.D., Oke, T.R., 2009. A new classification system for urban climate sites. Bull. Am. Meteorol. Soc. 90 (7), 922–923.
Stewart, I.D., Oke, T.R., 2012. Local climate zones for urban temperature studies. Bull. Am. Meteorol. Soc. 93 (12), 1879–1900. http://dx.doi.org/10.1175/bams-d-11-00019.1.
Stewart, Iain D., Oke, T.R., Scott Krayenhoff, E., 2014. Evaluation of the 'local climate zone' scheme using temperature observations and model simulations. Int. J. Climatol. 34 (4), 1062–1080. http://dx.doi.org/10.1002/joc.3746.
Stone, Brian, Hess, Jeremy J., Frumkin, Howard, 2010. Urban form and extreme heat events: are sprawling cities more vulnerable to climate change than compact cities. Environ. Health Perspect. 118 (10), 1425–1428.
Szymanowski, M., Kryza, M., 2009. GIS-based techniques for urban heat island spatialization. Clim. Res. 38 (2), 171–187.
Tan, Jianguo, Zheng, Youfei, Tang, Xu, Guo, Changyi, Li, Liping, Song, Guixiang, Zhen, Xinrong, Yuan, Dong, Kalkstein, Adam J., Li, Furong, Chen, Heng, 2010. The urban heat island and its impact on heat waves and human health in shanghai. Int. J. Biometeorol. 54 (1), 75–84. http://dx.doi.org/10.1007/s00484-009-0256-x.
Taylor, Bruce, 1986. Geography in Hong Kong. Prof. Geogr. 38 (4), 419–423. http://dx.doi.org/10.1111/j.0033-0124.1986.00419.x.
Tsin, Pak Keung, Anders, Knudby, Scott Krayenhoff, E., Ho, Hung Chak, Brauer, Michael, Henderson, Sarah B., 2016. Microscale mobile monitoring of urban air temperature. Urban Climate 18, 58–72. http://dx.doi.org/10.1016/j.uclim.2016.10.001.
Unger, János, Sümeghy, Zoltán, Zoboki, Judit, 2001. Temperature cross-section features in an urban area. Atmos. Res. 58 (2), 117–127. http://dx.doi.org/10.1016/S0169-8095(01)00087-4.
Unger, János, Stevan Savić, Tamás Mátyás Gál, Dragan Milošević, Enikő Lelovics, Vladimir Marković, Ágnes Gulyás, and Daniela Arsenović. 2015. Urban climate monitoring networks based on LCZ concept. In ICUC9 - 9th International Conference on Urban Climate jointly with 12th Symposium on the Urban Environment Toulouse, France.
Wang, Ran, Ren, Chao, Xu, Yong, Lau, Kevin Ka-Lun, Shi, Yuan, 2018. Mapping the local climate zones of urban areas by GIS-based and WUDAPT methods: a case study of Hong Kong. Urban Climate 24, 567–576. http://dx.doi.org/10.1016/j.uclim.2017.10.001.
WHO, 2003. Climate change and human health: risks and responses: summary. World Health Organization. Dept. of Protection of the Human Environment, Geneva.
Xu, Yong, Ren, Chao, Ma, Peifeng, Ho, Justin, Wang, Weiwen, Lau, Kevin Ka-Lun, Lin, Hui, Ng, Edward, 2017. Urban morphology detection and computation for urban climate research. In: Landscape and Urban Planning. 167 (Suppl. C). pp. 212–224. http://dx.doi.org/10.1016/j.landurbplan.2017.06.018.
Zheng, Y., Ren, C., Ng, E., Lau, K., Shi, Y., Ho, J.C.K., 2015. Spatial distribution of urban heat island and intra-urban air temperature variability in high-density urban areas in Hong Kong. In: 9th International Conference on Urban Climate. Toulouse, France: IAUC and AMS.
Zheng, Yingsheng, Ren, Chao, Xu, Yong, Wang, Ran, Ho, Justin, Lau, Kevin, Ng, Edward, 2018. GIS-based mapping of local climate zone in the high-density city of Hong Kong. Urban Climate 24, 419–448. http://dx.doi.org/10.1016/j.uclim.2017.05.008.